Biochemical and Biophysical Research Communications 447 (2014) 216–222

Contents lists available at ScienceDirect

Biochemical and Biophysical Research Communications

journal homepage: www.elsevier.com/locate/ybbrc

Androgen-independent proliferation of LNCaP prostate cancer cells infected by xenotropic murine leukemia virus-related virus

Katsura Kakoki [a,b,c], Haruka Kamiyama [a,b], Mai Izumida [a], Yuka Yashima [a], Hideki Hayashi [a], Naoki Yamamoto [b,d], Toshifumi Matsuyama [a], Tsukasa Igawa [c], Hideki Sakai [c], Yoshinao Kubo [a,b,*]

[a] Division of Cytokine Signaling, Graduate School of Biomedical Sciences, Nagasaki University, Nagasaki 852-8523, Japan
[b] Department of AIDS Research, Institute of Tropical Medicine, G-COE, Nagasaki University, Nagasaki 852-8523, Japan
[c] Department of Urology, Graduate School of Biomedical Sciences, Nagasaki University, Nagasaki 852-8523, Japan
[d] Department of Microbiology, National University of Singapore, Singapore

ARTICLE INFO

Article history:
Received 10 March 2014
Available online 8 April 2014

Keywords:
XMRV
LNCaP cell
Prostate cancer
Androgen

ABSTRACT

Xenotropic murine leukemia virus-related virus (XMRV) is a novel gammaretrovirus that was originally isolated from human prostate cancer. It is now believed that XMRV is not the etiologic agent of prostate cancer. An analysis of murine leukemia virus (MLV) infection in various human cell lines revealed that prostate cancer cell lines are preferentially infected by XMRV, and this suggested that XMRV infection may confer some sort of growth advantage to prostate cancer cell lines. To examine this hypothesis, androgen-dependent LNCaP cells were infected with XMRV and tested for changes in certain cell growth properties. We found that XMRV-infected LNCaP cells can proliferate in the absence of the androgen dihydrotestosterone. Moreover, androgen receptor expression is significantly reduced in XMRV-infected LNCaP cells. Such alterations were not observed in uninfected and amphotropic MLV-infected LNCaP cells. This finding explains why prostate cancer cell lines are preferentially infected with XMRV.

1. Introduction

Xenotropic murine leukemia virus-related retrovirus (XMRV) is a novel human gammaretrovirus that was originally isolated from human prostate cancer tissues [1]. Although it is widely believed at present that XMRV is not the etiologic agent of prostate cancer, human prostate cell lines are frequently infected with XMRV [2].

It is known that some retroviruses play a critical role in leukemogenesis in various mammalian species including human [3,4]. The xenotropic MLV infection receptor (XPR1), which is also recognized by XMRV [5,6], varies among wild mice species as a mechanism of resistance to xenotropic virus infection [7,8]. The latter observation suggests that xenotropic viruses may be pathogenic in some species and implies that XMRV may affect growth of certain cell lineages.

Prostate cancer cell lines exhibit a propensity for infection by XMRV when compared to other types of human cancer cell lines [2,9]. It has been reported that amyloidogenic fragments originating from prostatic acid phosphatase greatly increase XMRV infections of primary prostatic epithelial and stromal cells [10]. In vivo infection of macaques with XMRV has confirmed that prostate tissue has a high affinity for XMRV, and the prostate tissues remain continuously infected even after 5 months, when XMRV was undetectable in blood [11]. Dihydrotestosterone (DHT) stimulates XMRV expression in cells expressing a functional androgen receptor (AR) [12,13]. These results suggest that XMRV infection specifically confers an advantage to prostate cancer cells.

In this study, we aimed to determine whether XMRV infection affects androgen-dependent growth of the LNCaP human prostate cancer cell line. Our results indicate that XMRV infection may provide an androgen-independent growth advantage to prostate cancer cells.

2. Materials and methods

2.1. Cells

PC-3 and LNCaP cells were obtained from ATCC. PC-3 cells were cultured in RPMI 1640 medium (Wako) supplemented with 8% (v/v) fetal bovine serum (FBS) (Biofuies), L-glutamine and penicillin–streptomycin (both from Sigma–Aldrich). LNCaP cells [14] were maintained in the same medium but additionally supplemented with 10 nM dihydrotestosterone (DHT) (Sigma–

* Corresponding author at: Division of Cytokine Signaling, Graduate School of Biomedical Sciences, Nagasaki University, 1-12-4 Sakamoto, Nagasaki 852-8523, Japan.
E-mail address: yoshinao@nagasaki-u.ac.jp (Y. Kubo).

http://dx.doi.org/10.1016/j.bbrc.2014.03.154
0006-291X/

Aldrich). Rat F10, human HeLa, and human 293T cells were cultured in Dulbecco's modified Eagle's medium supplemented with 8% FBS and penicillin–streptomycin. All cell lines were grown in a tissue culture incubator at 37 °C with a 5% CO_2 atmosphere.

2.2. Retrovirus infection

The XMRV plasmid DNA was obtained from Dr. R.H. Silverman and Dr. B. Dong [1] through the AIDS Research and Reference Reagent Program (NIAID, NIH, USA) and was used for transfection of rat F10 cells. Culture supernatants of transfected F10 cells were used to inoculate target cells in presence of polybrene (4 μg/ml) (Sigma). Inocula containing MLV were from culture supernatants of amphotropic MLV-producing cells, obtained from Dr. Y. Iwatani. Infected LNCaP cells were maintained in presence of DHT. In tests of androgen responses, target cells were cultured in various combinations of DHT (10 nM) and bicalutamide (10 μM).

2.3. Cell counts and viability

The cells to be counted were collected and stained with trypan blue. Numbers of unstained (viable) cells were counted using a counting chamber under a microscope to estimate cell viability.

2.4. Western blot analysis

Cell lysates were subjected to electrophoretic separation in SDS-containing polyacrylamide gels (BioRad), after which proteins were transferred onto a PVDF membrane. The membrane was first treated with the primary antibodies: mouse anti-β-actin (Santa Cruz Biotechnology), goat anti-dynamin (Santa Cruz Biotechnology), rabbit anti-human AR (Santa Cruz Biotechnology), goat anti-MLV p30 Gag (ViroMed), or goat anti-MLV SU (ViroMed) antibody. Following these procedures, the membrane was treated with secondary horse radish peroxidase (HRP)-conjugated anti-mouse IgG antibody, or HRP-conjugated protein G (Bio-Rad). Secondary antibody- or protein G-bound polypeptides were detected by ECL Western Blotting Detection Reagents (GE healthcare).

2.5. Semi-quantitative RT-PCR

Total RNA and genomic DNA samples were isolated by standard protocols. Fist-strand cDNA was synthesized using reverse transcriptase (TaKaRa) from the total RNA (500 ng). Semiquantitative PCR was performed to detect XMRV env, AR, and GAPDH sequences. Nucleotide sequences of the PCR primers for the XMRV *env* sequences were 5′-GACTTGTGTGATTTAGTTGGAGAC-3′ and 5′-CCCCGGTGTGGCACC-3′; for AR, 5′-AGCCCCACTGAGACAACC-3′ and 5′-ATCAGGGGCGAAGTAGAGCAT-3′; and for GAPDH, 5′-AGG TXGGAGTXAAXGGATTTGGT-3′ and 5′-GTGGGCCATGAGGATCCAC-CAC-3′. These primers were synthesized by Genenet Inc.

2.6. Statistical analysis

Differences between two sets of data were determined by Student's *t*-test, and these differences were considered significant when $P < 0.05$.

3. Results

3.1. XMRV infection converts LNCaP cells to an androgen-independent phenotype

To analyze the effect of XMRV infection on androgen-dependent growth of LNCaP cells, the proliferation of XMRV-infected and -uninfected LNCaP cells was compared. As it has been reported that XMRV can replicate in rat cells but not in human 293T cells [12,13,], virus was first rescued by transfection of an XMRV expression plasmid [1] in rat F10 cells. Undiluted culture supernatant from these cells was then added to LNCaP cells with polybrene and cultured for 24 h. The XMRV-infected and -uninfected cells were maintained in the presence of 10 nM DHT for more than 3 months. Uninfected LNCaP cells did not grow in the absence of DHT (Fig. 1A) but did in the presence of DHT (Fig. 1B), indicating a strong androgen-dependent growth requirement, as reported [14]. As a control for specific AR effects, DHT-induced growth of uninfected LNCaP cells was shown to be abrogated by the antagonist bicalutamide, an androgen blocker (Fig. 1C). Bicalutamide (10 μM) alone had no effect on the growth of either infected or uninfected LNCaP cells (Fig. 1D). LNCaP cells chronically infected with XMRV grew even in the absence of DHT (Fig. 1A), and bicalutamide did not suppress growth of XMRV-infected LNCaP cells (Fig. 1C and D). In the presence of DHT, the number of XMRV-infected LNCaP cells was greater than control uninfected cells after 3 days in culture (Fig. 1B). Three independent XMRV-infected LNCaP cell pools were constructed, and all of them could grow in the absence of DHT. When uninfected LNCaP cells were maintained in the presence of DHT, the cells did not gain androgen-independent growth property during this study. These results indicate that XMRV infection converts LNCaP cell growth from androgen dependence to independence.

On the other hand, LNCaP cells chronically infected with amphotropic MLV did not efficiently proliferate even in the presence of DHT (Fig. 1A–D), suggesting that the amphotropic MLV infection is cytotoxic for LNCaP cells.

To determine the time course of the conversion of XMRV-infected LNCaP cells to androgen independence, growth kinetics were analyzed after XMRV infection (from 1 to 2 months, 2 to 3 months, and >3 months). Cultures initially contained 5×10^3 cells and were counted again after 6 days, because differences between the uninfected and XMRV-infected LNCaP cells in androgen dependence were apparent 6 days after the culture was started (Fig. 1A–D). DHT dependence of LNCaP cell growth was reduced by XMRV infection, but DHT still activated cell proliferation 1–2 months after XMRV infection (Fig. 1E). Cell numbers of the infected LNCaP cells in the absence of DHT were comparable to those in its presence 2–3 months after infection. These results suggest that the complete conversion of LNCaP cells to androgen independence takes more than 2 months. The XMRV infection did not increase cell numbers in the absence of DHT 1–3 months after the XMRV inoculation, but cell increases were observed longer than 3 months after inoculation, showing that the activation of LNCaP cell growth by the XMRV infection requires at least 3 months.

Uninfected PC-3 cells, whose growth is androgen-independent [15], grew as efficiently as XMRV-infected PC-3 cells in the absence or presence of DHT (data not shown). These results indicate that XMRV infection did not affect growth of androgen-independent PC-3 cells.

3.2. XMRV infection inhibits androgen receptor expression in LNCaP cells

Because androgen agonistic (DHT) and antagonistic (bicalutamide) effects are mediated through androgen receptor (AR), we analyzed the effects of XMRV infection on its expression in LNCaP cells. As demonstrated by western blot analysis, the expression of AR protein gradually decreased after XMRV infection of LNCaP cells (Fig. 2A). Expression was significantly decreased but still detectable 2–3 months after infection, but by >3 months no expression was observed. Therefore, the reduction of AR

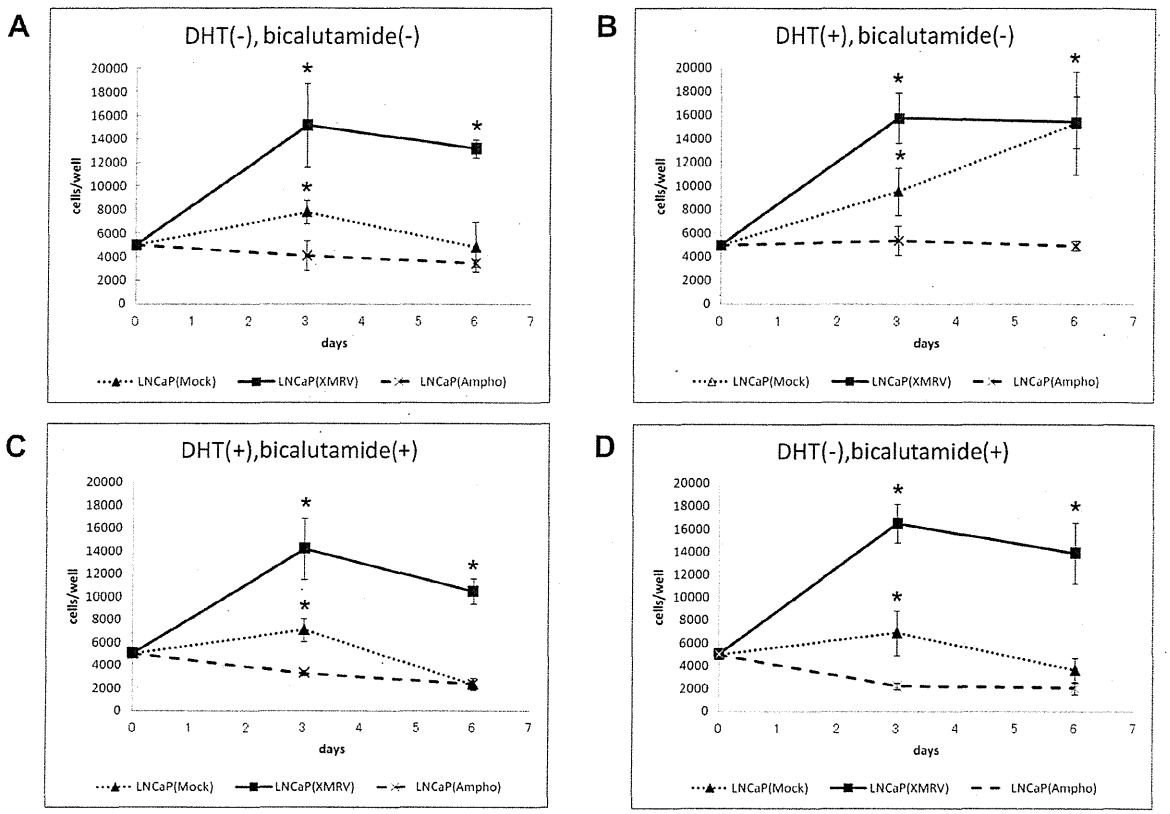

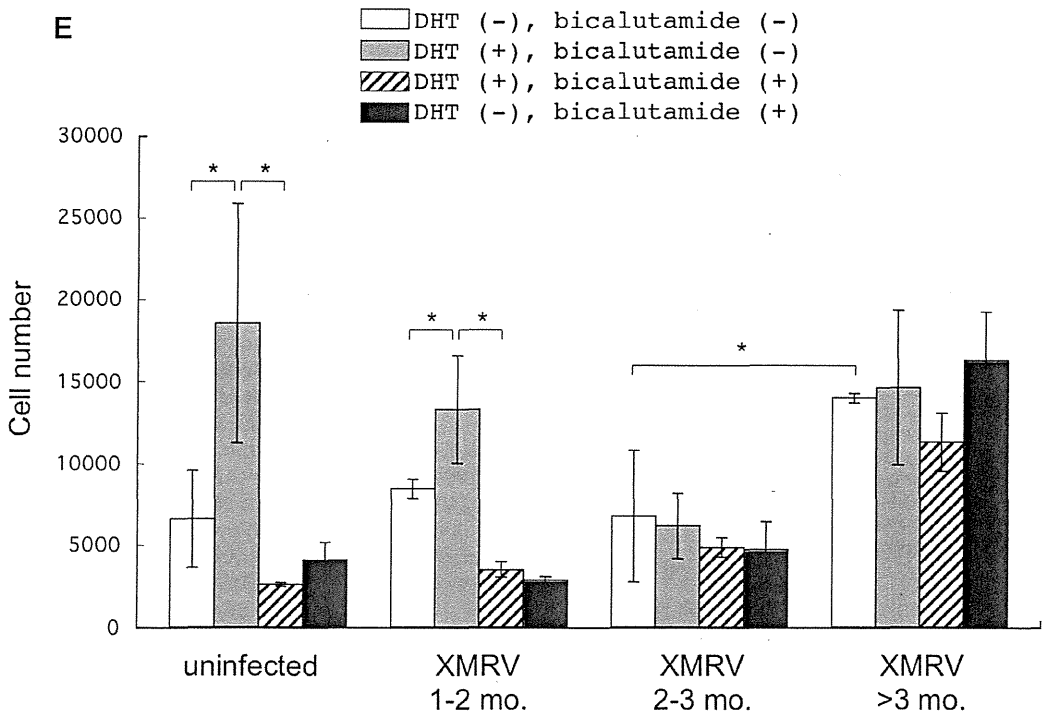

Fig. 1. XMRV infection converts the phenotype of LNCaP cells from androgen-dependent to androgen-independent. (A–D) Growth of uninfected, chronically XMRV-infected, and amphotropic MLV-infected LNCaP cells cultured in media supplemented with or without the androgen dihydrotestosterone (DHT) and/or the androgen receptor antagonist bicalutamide. (E) Effects of DHT and bicalutamide on growth of uninfected and XMRV-infected LNCaP cells were analyzed. Cells were counted after 6 days in culture. In all the panels, the data presented are average values ± SD from two independent experiments performed in triplicate. The concentrations of DHT used in the experiments were (+) 10 nM, or (−) 0 nM; and of bicalutamide, (+) 10 μM, or (−) 0 μM.

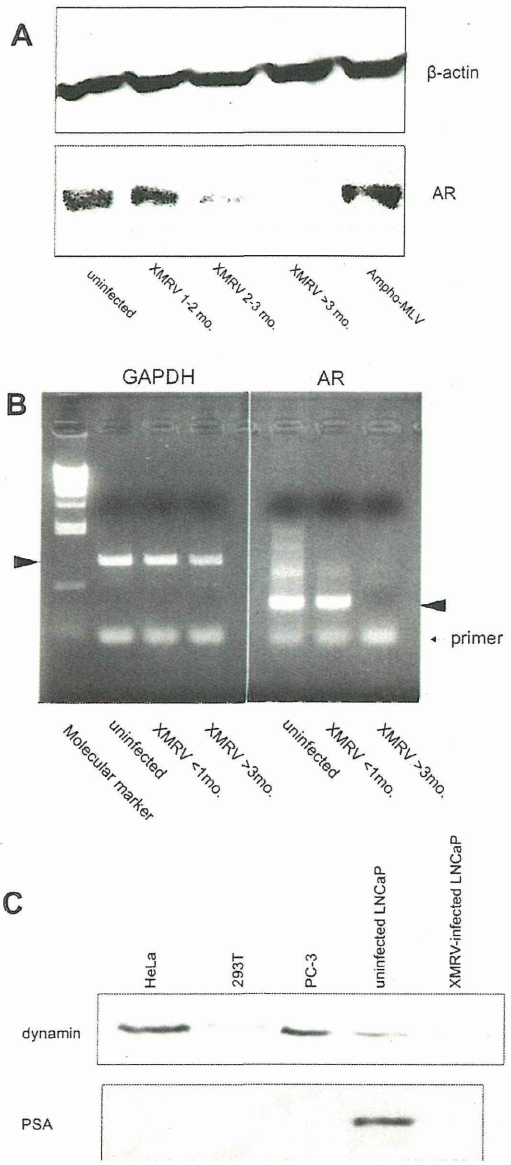

Fig. 2. XMRV infection results in reduced androgen receptor (AR) protein and mRNA expression. (A) Results of western blot analysis of cell lysates from uninfected, XMRV-infected (at three time points after infection, indicated below the chart), and amphotropic MLV-infected LNCaP cells. Levels of AR (lower panel) and β-actin protein expression (internal positive control, in upper panel) are shown. (B) AR and GAPDH mRNA expression levels from uninfected and XMRV-infected LNCaP cells analyzed by semiquantitative RT-PCR. Arrow heads indicate predicted sizes of the PCR products. (C) PSA protein expression was analyzed in HeLa, 293T, PC-3, uninfected LNCaP, and XMRV-infected LNCaP cells by western blot. As control, dynamin expression was also examined.

expression occurred in parallel with the conversion to androgen-independent proliferation. In LNCaP cells chronically infected with amphotropic MLV, AR expression was not affected (last lane of Fig. 2A).

To determine whether the reduction of AR protein expression by XMRV infection was associated with decreased AR transcript levels, we examined mRNA expression by semiquantitative RT-PCR. As the result, we found that the AR mRNA level in LNCaP cells is counteracted by the XMRV infection (Fig. 2B). These findings demonstrated that the XMRV infection induces the androgen-independent growth and attenuates the AR gene transcription in LNCaP cells.

LNCaP cells have been shown to exhibit androgen-dependent expression of the prostate-specific antigen (PSA) [14]. We therefore analyzed PSA expression in LNCaP cells converted to androgen independence by XMRV. PSA expression was not detected in HeLa, 293T, or androgen-independent PC-3 prostate cancer cells (Fig. 2C). Uninfected LNCaP cells expressed PSA, but chronically XMRV-infected LNCaP cells did not, even though the cells were cultured in the presence of DHT.

3.3. The expression of XMRV proteins depends on androgen stimulation

Because it has been reported that XMRV expression is dependent on androgen and AR [12,13], we analyzed XMRV Gag and Env protein expression in infected LNCaP cells. Our results show that expression of XMRV Gag gradually decreased after infection, correlating with the time course of conversion to androgen-independent growth (Fig. 3A). Three months after XMRV infection, both the Gag precursor and mature protein levels were much lower than after 1–2 month. The XMRV Env protein was expressed for as long as 3 months after infection, but at periods longer than 3 months expression was not detected (Fig. 3B).

Amount of XMRV sequence integrated into genomes of chronically infected LNCaP cells were comparable to that at shorter than 1 month (Fig. 4A), indicating that XMRV-infected cells were maintained during the culture. XMRV RNA level at periods longer than 3 months after XMRV infection was lower than that at shorter than 1 month (Fig. 4B). These results indicate that XMRV expression is reduced during LNCaP cell phenotypic conversion and support the conclusion that XMRV expression is dependent on androgen [12,13].

The XMRV Gag proteins were not detected by western analysis of XMRV-infected PC-3 cells (Fig. 3A), but the XMRV env sequence-containing RNA was detected by RT-PCR (Fig. 4C), showing that XMRV genome was integrated and transcribed at low level in PC-3 cells. Because PC-3 cells are androgen-independent and lack AR expression [16], the androgen-dependent XMRV Gag protein level was presumably below detectable limits (Fig. 3A). In contrast, Gag protein was detected by western analysis in LNCaP cells chronically infected with amphotropic MLV (Fig. 3A), showing that the amphotropic MLV expression was independent of androgen.

4. Discussion

In this study, we found that XMRV infection converts the androgen-dependent phenotype of LNCaP cells to androgen independence, and it reduces AR expression. This effect seems to be relatively specific to XMRV, as it was not observed with amphotropic MLV infection of the same cells. Consistently, it has been reported that XMRV activates tumor growth and invasiveness of LNCaP cells [17–19], but androgen dependence of LNCaP cell proliferation was not analyzed in these studies. Many human cancer cells have been transplanted into nude mice, but prostate cancer cells are preferentially infected with xenotropic MLVs [2]. The XMRV-mediated androgen-independent growth of prostate cancer cells may explain the propensity for XMRV infection observed in prostate cancer cells.

It has been reported that androgen-independent LNCaP cells spontaneously appear during culture in the absence of androgen [14,20]. However, XMRV-infected LNCaP cells became androgen-independent even in the presence of androgen. Because the XMRV infection suppressed AR protein expression, DHT cannot induce growth activation. Indeed, less than 3 months after the XMRV infection, growth of the infected LNCaP cells was not activated even in the presence of DHT. Then, spontaneous alterations inducing androgen-independent growth might be selected in the

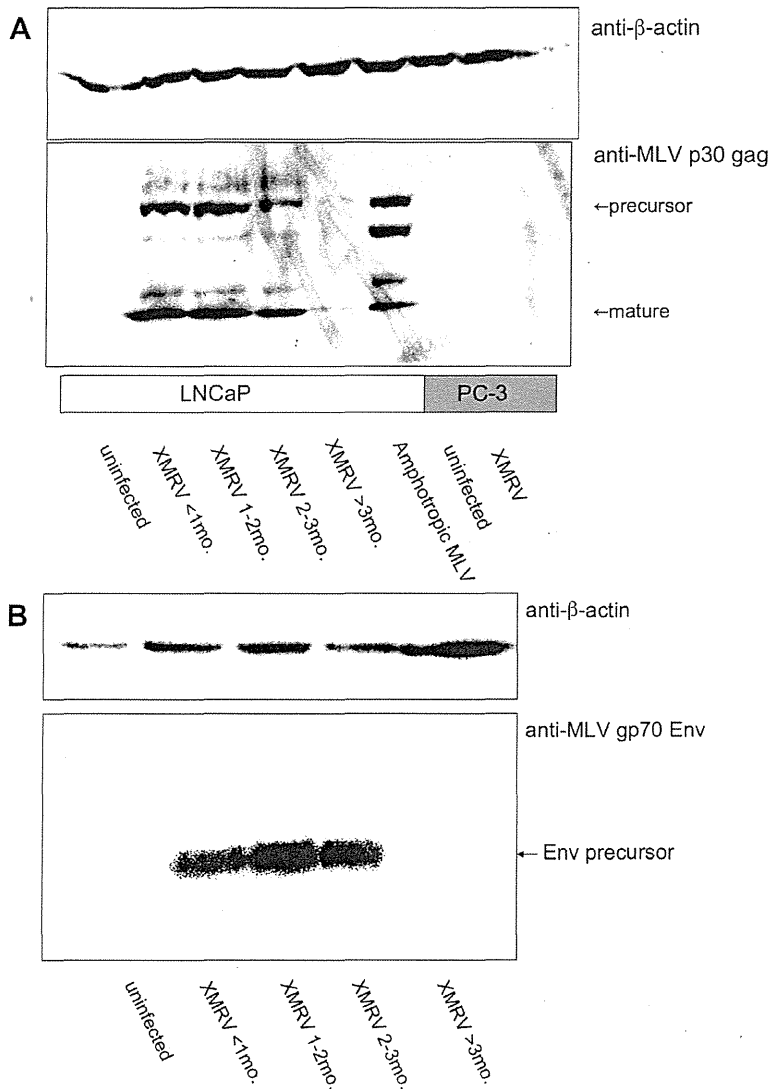

Fig. 3. XMRV expression was decreased in parallel with XMRV-induced conversion of LNCaP cells from androgen-dependent to -independent growth. Western blot analysis of MLV Gag (panel A) and Env (panel B) protein levels were evaluated in uninfected, amphotropic MLV-infected, and XMRV-infected LNCaP, and PC-3 cells. As a positive internal control, β-actin protein expression levels were also analyzed.

XMRV-infected LNCaP cell culture. Because the expression of XMRV proteins was suppressed in chronically XMRV-infected LNCaP cells, the viral proteins are not necessary for maintenance of the androgen-independent state. This observation supports the above speculation. If so, the XMRV infection did not directly induce the androgen-independent growth. However, the abrogation of AR expression by the XMRV infection triggered the conversion to androgen-independent growth.

How does XMRV reduce AR expression? Amphotropic MLV infection inhibited growth of LNCaP cells. Thus, though the XMRV infection did not clearly suppress the cell growth, XMRV proteins may be slightly toxic to LNCaP cells. Because XMRV expression is androgen-dependent, lower level of AR expression induces lower amount of XMRV proteins. Due to this mechanism, LNCaP cells expressing AR at lower level might be selected during the culture. Further study is required to understand the mechanism by which XMRV infection abrogates AR protein expression.

The expression of XMRV was reduced in the androgen-independent XMRV-infected LNCaP cells. However, xenotropic MLVs are constitutively expressed in the androgen-independent CWR22Rv1 prostate cancer cells [9] and in several human cancer cell lines other than prostate cancer [21–23]. These results indicate that expression of these xenotropic MLVs is independent of androgen.

As a clinical problem, most prostate cancer patients treated with combined androgen blockage (CAB) therapy develop castration resistant prostate cancer (CRPC) [24]. Growth of the prostate cancer cells is androgen-dependent in the first stage, and thereafter androgen-independent cancer cells are selected during CAB therapy. The androgen refractory mechanisms are explained by the following hypotheses [24]: (i) mutations in or enhanced expression of the AR gene; (ii) mutated AR is activated by other steroids; (iii) mutated AR is activated by other signals, e.g., peptide growth factors or cytokines; or (iv) an AR bypassing pathway is activated. Mechanisms of the fourth case are not completely understood, and it is to this category that XMRV-induced conversion belongs. This is because AR expression is significantly reduced in XMRV-infected LNCaP cells. The mechanism of AR-deficient CRPC development in human patients may be similar to that of the XMRV-induced LNCaP androgen independence. Elucidation of the mechanism by which XMRV induces

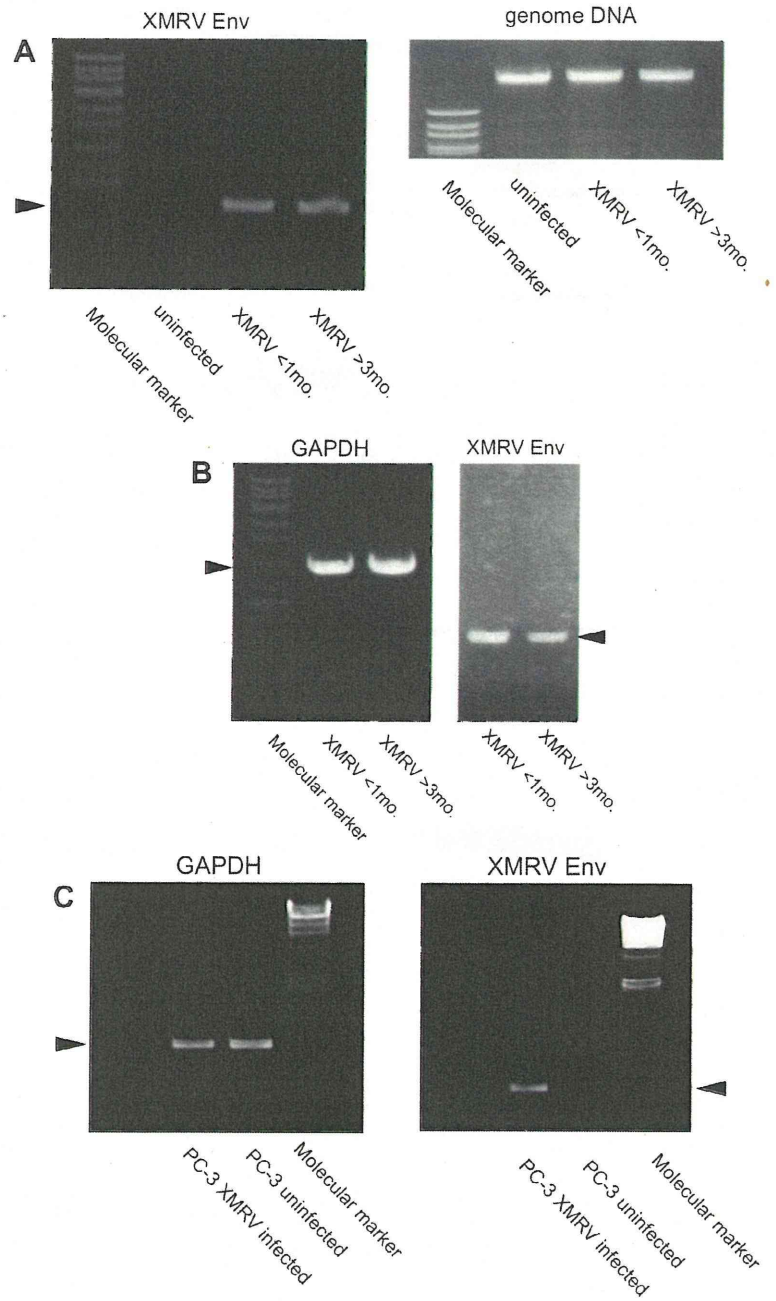

Fig. 4. XMRV transcription was decreased in XMRV-infected LNCaP cells. (A) XMRV sequences integrated into LNCaP cell genomes were detected by PCR (left panel). Equal amounts of genomic DNAs (500 ng) were analyzed (right panel). (B) Levels of XMRV env mRNA was quantified by RT-PCR in XMRV-infected LNCaP cells. (C) XMRV env mRNA levels was measured in uninfected and XMRV-infected PC-3 cells (right panel). As control, GAPDH mRNA was analyzed in the same samples (left panel). Arrow heads indicate predicted sizes of the PCR products.

androgen-independent growth of LNCaP cells would contribute to a more complete understanding of CRPC development and novel therapies for human prostate cancer patients.

Acknowledgments

We thank Dr. Silvermann and Dr. B. Dong for the XMRV DNA clone and Dr. Y. Iwatani for amphotropic MLV. We also thank Ms. M. Haraguchi, Ms. Y. Kobayashi, and Ms. F. Tsujita for assistance. This study was partially supported by the Japan Society for the Promotion of Science (JSPS) (No. 09J07637).

References

[1] A. Urisman, R.J. Molinaro, N. Fischer, S.J. Plummer, G. Casey, E.A. Klein, K. Malathi, C. Magi-Galluzzi, R.R. Tubbs, D. Ganem, R.H. Silverman, J.L. DeRisi, Identification of a novel gammaretrovirus in prostate tumors of patients homozygous for R462Q RNASEL variant, PLoS Pathog. 2 (2006) e25.
[2] K.S. Stanos, A.L. Alota, J.L. Hicks, D.M. Esopi, J.P. Steranka, W. Shao, S. Sanchez-Martinez, S. Yegnasubramanian, K.H. Burns, A. Rein, A.M. De Marzo, Identification of replication competent murine gammaretroviruses in commonly used prostate cancer cell lines, PLoS One 6 (2011) e20874.
[3] H. Fan, Leukemogenesis by Moloney murine leukemia virus: a multistep process, Trends Microbiol. 5 (1997) 74–82.
[4] M. Matsuoka, Human T-cell leukemia virus type I (HTLV-I) infection and the onset of adult T-cell leukemia (ATL), Retrovirology 2 (2005) 27.

[5] J.L. Battini, J.E. Rasko, A.D. Miller, A human cell-surface receptor for xenotropic and polytropic murine leukemia viruses: possible role in G protein-coupled signal transduction, Proc. Natl. Acad. Sci. U.S.A. 96 (1999) 1385–1390.
[6] S. Bhosle, S. Suppiah, R. Molinaro, Y. Liang, R. Arnold, W. Diehl, N. Makarova, J. Blackwell, J. Petros, D. Liotta, E. Hunter, H. Ly, Evaluation of cellular determinants required for in vitro xenotropic murine leukemia virus-related virus entry into human prostate cancer and noncancerous cells, J. Virol. 84 (2010) 6288–6296.
[7] Y. Yan, R.C. Knöper, C.A. Kozak, Wild mouse variants of envelope genes of xenotropic/polytropic mouse gammaretroviruses and their XPR1 receptors elucidate receptor determinants of virus entry, J. Virol. 81 (2007) 10550–10557.
[8] Y. Yan, Q. Liu, K. Wollenberg, C. Martin, A. Buckler-White, C.A. Kozak, Evolution of functional and sequence variants of the mammalian XPR1 receptor for mouse xenotropic gammaretroviruses and the human-derived retrovirus XMRV, J. Virol. 84 (2010) 11970–11980.
[9] E.C. Knouf, M.J. Metzger, P.S. Mitchell, J.D. Arroyo, J.R. Chevillet, M. Tewari, A.D. Miller, Multiple integrated copies and high-level production of the human retrovirus XMRV (xenotropic murine leukemia virus-related virus) from 22Rv1 prostate carcinoma cells, J. Virol. 83 (2009) 7353–7356.
[10] S. Hong, E.A. Klein, J. Das Gupta, K. Hanke, C.J. Weight, C. Nguyen, C. Gaughan, K.A. Kim, N. Bannert, F. Kirchhoff, J. Munch, R.H. Silverman, Fibrils of prostatic acid phosphatase fragments boost infections with XMRV (xenotropic murine leukemia virus-related virus), a human retrovirus associated with prostate cancer, J. Virol. 83 (2009) 6995–7003.
[11] N. Onlamoon, J. Das Gupta, P. Sharma, K. Rogers, S. Suppiah, J. Rhea, R.J. Molinaro, C. Gaughan, B. Dong, E.A. Klein, X. Qiu, S. Devare, G. Schochetman, J. Hackett, R.H. Silverman, F. Villinger, Infection, viral dissemination, and antibody responses of rhesus macaques exposed to the human gammaretrovirus XMRV, J. Virol. 85 (2011) 4547–4557.
[12] B. Dong, R.H. Silverman, Androgen stimulates transcription and replication of xenotropic murine leukemia virus-related virus, J. Virol. 84 (2010) 1648–1651.
[13] J.J. Rodriguez, S.P. Goff, Xenotropic murine leukemia virus-related virus establishes an efficient spreading infection and exhibits enhanced transcriptional activity in prostate carcinoma cells, J. Virol. 84 (2010) 2556–2562.
[14] T. Igawa, F.F. Lin, M.S. Lee, D. Karan, S.K. Batra, M.F. Lin, Establishment and characterization of androgen-independent human prostate cancer LNCaP cell model, Prostate 50 (2002) 222–235.
[15] M. Igawa, D.B. Rukstalis, T. Tanabe, G.W. Chodak, High levels of nm23 expression are related to cell proliferation in human prostate cancer, Cancer Res. 54 (1994) 1313–1318.
[16] T. Demura, N. Kuzumaki, A. Oda, H. Fujita, T. Ishibashi, T. Koyanagi, Establishment and characterization of monoclonal antibody against androgen receptor, J. Steroid. Biochem. 33 (1989) 845–851.
[17] J. Pandhare-Dash, C.K. Mantri, Y. Gong, Z. Chen, C. Dash, XMRV accelerates cellular proliferation, transformational activity, and invasiveness of prostate cancer cells by downregulating p27 (Kip1), Prostate 72 (2012) 886–897.
[18] M. Murgai, J. Thomas, O. Cherepanova, K. Delviks-Frankenberry, P. Deeble, V.K. Pathak, D. Rekosh, G. Owens, Xenotropic MLV envelope proteins induce tumor cells to secrete factors that promote the formation of immature blood vessels, Retrovirology 10 (2013) 34.
[19] K. Stieler, U. Schumacher, A.K. Horst, N. Fischer, XMRV induces cell migration, cytokine expression and tumor angiogenesis: are 22Rv1 cells a suitable prostate cancer model?, PLoS One 7 (2012) e42321.
[20] T.C. Yuan, S. Veeramani, F.F. Lin, D. Kondrikou, S. Zelivianski, T. Igawa, D. Karan, S.K. Batra, M.F. Lin, Androgen deprivation induces human prostate epithelial neuroendocrine differentiation of androgen-sensitive LNCaP cells, Endocr. Relat. Cancer 13 (2006) 151–167.
[21] J.L. Cmarik, J.A. Troxler, C.A. Hanson, X. Zhang, S.K. Ruscetti, The human lung adenocarcinoma cell line EKVX produces an infectious xenotropic murine leukemia virus, Viruses 3 (2011) 2442–2461.
[22] K.P. Raisch, M. Pizzato, H.Y. Sun, Y. Takeuchi, L.W. Cashdollar, S.E. Grossberg, Molecular cloning, complete sequence, and biological characterization of a xenotropic murine leukemia virus constitutively released from the human B-lymphoblastoid cell line DG-75, Virology 308 (2003) 83–91.
[23] Y.A. Zhang, A. Maitra, J.T. Hsieh, C.M. Rudin, C.D. Peacock, C. Karikari, R.A. Brekken, V. Stastny, B. Gao, L. Girard, I. Wistuba, E. Frenkel, J.D. Minna, A.F. Gazdar, Frequent detection of infectious xenotropic murine leukemia virus (XMLV) in human cultures established from mouse xenografts, Cancer Biol. Ther. 12 (2011) 617–628.
[24] T. Inoue, O. Ogawa, Role of signaling transduction pathways in development of castration-resistant prostate cancer, Prostate Cancer 2011 (2011) 647987.

Virus Genes (2014) 48:448–456
DOI 10.1007/s11262-014-1036-1

Susceptibility of muridae cell lines to ecotropic murine leukemia virus and the cationic amino acid transporter 1 viral receptor sequences: implications for evolution of the viral receptor

Katsura Kakoki · Akio Shinohara · Mai Izumida · Yosuke Koizumi · Eri Honda · Goro Kato · Tsukasa Igawa · Hideki Sakai · Hideki Hayashi · Toshifumi Matsuyama · Tetsuo Morita · Chihiro Koshimoto · Yoshinao Kubo

Received: 22 October 2013 / Accepted: 9 January 2014 / Published online: 28 January 2014

Abstract Ecotropic murine leukemia viruses (Eco-MLVs) infect mouse and rat, but not other mammalian cells, and gain access for infection through binding the cationic amino acid transporter 1 (CAT1). Glycosylation of the rat and hamster CAT1s inhibits Eco-MLV infection, and treatment of rat and hamster cells with a glycosylation inhibitor, tunicamycin, enhances Eco-MLV infection. Although the mouse CAT1 is also glycosylated, it does not inhibit Eco-MLV infection. Comparison of amino acid sequences between the rat and mouse CAT1s shows amino acid insertions in the rat protein near the Eco-MLV-binding motif. In addition to the insertion present in the rat CAT1, the hamster CAT1 has additional amino acid insertions. In contrast, tunicamycin treatment of mink and human cells does not elevate the infection, because their CAT1s do not have the Eco-MLV-binding motif. To define the evolutionary pathway of the Eco-MLV receptor, we analyzed CAT1 sequences and susceptibility to Eco-MLV infection of other several murinae animals, including the southern vole (*Microtus rossiaemeridionalis*), large Japanese field mouse (*Apodemus speciosus*), and Eurasian harvest mouse (*Micromys minutus*). Eco-MLV infection was enhanced by tunicamycin in these cells, and their CAT1 sequences have the insertions like the hamster CAT1. Phylogenetic analysis of mammalian CAT1s suggested that the ancestral CAT1 does not have the Eco-MLV-binding motif, like the human CAT1, and the mouse CAT1 is thought to be generated by the amino acid deletions in the third extracellular loop of CAT1.

Keywords Ecotropic murine leukemia virus · CAT1 · Glycosylation · Evolution

K. Kakoki · M. Izumida · Y. Koizumi · E. Honda · H. Hayashi · T. Matsuyama · Y. Kubo (✉)
Division of Cytokine Signaling, Graduate School of Biomedical Sciences, Nagasaki University, 1-12-4 Sakamoto, Nagasaki 852-8523, Japan
e-mail: yoshinao@nagasaki-u.ac.jp

K. Kakoki · T. Igawa · H. Sakai
Department of Urology, Graduate School of Biomedical Sciences, Nagasaki University, Nagasaki 852-8523, Japan

A. Shinohara · G. Kato · C. Koshimoto
Division of Biotechnology, Department of Bio-resources, Frontier Science Research Center, University of Miyazaki, Miyazaki 889-1692, Japan

T. Morita
Department of Plant and Animal Science, Faculty of Agriculture, University of Miyazaki, Miyazaki 889-2192, Japan

Y. Kubo
Department of AIDS Research, Institute of Tropical Medicine, G-COE, Nagasaki University, Nagasaki 852-8523, Japan

Introduction

A change in the cell surface receptor for a virus is one of a host defense mechanism against virus infection; for example, the C-terminally truncated CCR5 variant is known to confer resistance to human immunodeficiency virus (HIV) infection [1]. We have analyzed the viral receptors for ecotropic murine leukemia viruses (Eco-MLVs) in mouse (*Mus musculus*), rat (*Ratus norvegicus*), and *Mus dunni* cells as a model of receptor evolution that confers resistance to a virus infection [2–4].

Eco-MLVs can infect mouse and rat cells, and recognize the multi-membrane-spanning cationic amino acid transporter 1 (CAT1) as the receptor for infection [5]. Eco-MLV binds the YGE or HGE motif in the third extracellular loop of the CAT1 [6, 7]; the CAT1 has two N-linked

glycosylation sites near the Eco-MLV-binding motif. Nucleotide sequences near the virus-binding motif are highly diversified among mouse, rat, hamster, mink, and human, suggesting that the region is under selective pressure.

Rat cells are much less susceptible to Eco-MLV infection than mouse cells, and hamster cells are completely resistant to infection. Treatment of rat and hamster cells with tunicamycin, an N-linked glycosylation inhibitor, enhances susceptibility to Eco-MLV infection [8, 9]. Furthermore, an amino acid substitution at the glycosylation site of the rat CAT1 increases susceptibility to Eco-MLV infection [2]. These results indicate that N-linked glycosylation of the rat and hamster CAT1 proteins inhibits Eco-MLV infection. Although the mouse CAT1 is also glycosylated at the same amino acid residues as the rat and hamster CAT1s, it does not affect Eco-MLV infection [2]; rat and hamster CAT1 proteins have three- and six-amino acid insertions near the viral-binding domain of the protein compared to the mouse CAT1. We have previously reported that a deletion of the amino acid insertion in the rat CAT1 confers increased susceptibility, and abrogates the glycosylation-mediated inhibition of Eco-MLV infection, indicating that the amino acid insertion in the rat CAT1 is the determinant for the glycosylation-dependent infection inhibition [3]. The longer insertion present in the hamster CAT1 compared to the rat protein may confer hamster cells a complete resistance to Eco-MLV infection. In addition, glycosylation of the *Mus dunni* CAT1 also inhibits Eco-MLV infection as a result of a one-amino acid insertion in the YGE virus-binding motif [4].

To confirm the pathway of evolution for mammalian CAT1s, we established immortalized cell lines from several murinae animals, and then determined their susceptibility to Eco-MLV infection and their CAT1 sequences. We showed that the CAT1 sequences of the southern vole, large Japanese field mouse, and Eurasian harvest mouse were shown to have amino acid insertions similar to the hamster CAT1. Phylogenetic analysis of mammalian CAT1 sequences revealed that the CAT1 ancestor is the human-type CAT1, and evolved to the mouse-type CAT1 by deletion rather than by insertion. This study reviews the evolutionary pathway of the ecotropic MLV receptor, CAT1, in relation to the viral infection.

Materials and methods

Animals

The southern vole (*Microtus rossiaemeridionalis*) and steppe lemming (*Lagurus lagurus*) were obtained from the closed colony maintained at the Frontier Science Research Center, University of Miyazaki. The Mongolian gerbil (*Meriones unguiculatus*) was obtained from the closed colony maintained at the Institute of Tropical Medicine, Nagasaki University. A wild large Japanese field mouse (*Apodemus speciosus*) and a Eurasian harvest mouse (*Micromys minutus*) were captured in Kiyotake, Miyazaki City, Miyazaki Prefecture, Japan, with the approval of the prefectural governor (No. 24940-2696). This animal study is approved by the Ethics Committee of Nagasaki University (No. 0812080723), and the Committee for the Ethics on Animal Experiments at the University of Miyazaki (No. 2008-505).

Cells

Mouse NIH3T3, rat F10, and human TELCeB6 [10] cells were cultured in Dulbecco's modified Eagle's medium (D-MEM) supplemented with 8 % fetal bovine serum (FBS). Kidney grafts of *M. minutus*, *M. rossiaemeridionalis,* and muscle grafts of *A. speciosus* were isolated and were treated with trypsin to separate cells. The cells were cultured with D-MEM containing 20 % FBS for more than one year. Cells from *M. rossiaemeridionalis* and *A. speciosus* were passed by 1/6 dilution every 3 days. Cells from *M. minutus* were passed by 1/2 dilution every 6 days.

Expression plasmids

An expression plasmid of the ecotropic Friend MLV Env has been already described [11]. A VSV-G expression plasmid was obtained from Dr. L. Chang through the AIDS Research and Reference Reagent Program, NIAID, NIH, USA [12].

Transduction assay

TELCeB6 cells [10] were transfected with an expression plasmid containing the Friend MLV envelope protein using the Fugene transfection reagent (Promega). Since the expression plasmid also encodes the neomycin resistance gene, the transfected cells were selected by geneticin (Invitrogen). Culture supernatants of the geneticin-resistant cell pool were inoculated into target cells in the presence of Polybrene (4 μg/ml) (Sigma–Aldrich). To construct a VSV-pseudotyped MLV vector, TELCeB6 cells were transiently transfected with a VSV-G expression plasmid and their culture supernatants were collected 2 days after transfection. The culture supernatants were then inoculated into target cells. To estimate transduction titer, the inoculated cells were stained with 5-bromo-4-chloro-3-indolyl-β-D-galactopyranoside (X-Gal) (Wako) 2 days after the inoculation and then blue cells were counted.

Isolation of CAT1 sequences

Total RNA samples were prepared from cells using Isogen (Invitrogen). cDNAs were synthesized by reverse transcriptase (TaKaRa) and a fragment containing the third extracellular loop of CAT1 and its upstream region was amplified by PCR (TaKaRa) using the cDNA as template. Nucleotide sequences of the PCR primers are AAC CTG ATT CTC TCC TAC ATC and GTG GTG GCG ATG CAG TCA AAG. The PCR products were cloned into pTarget vector (Promega) and nucleotide sequences of the insert DNAs were determined (Applied Biosystems). The primers were synthesized by Genenet Co., LTD. Accession numbers of CAT1s from A. speciosus, *M. rossiaemeridionalis,* and *M. minutus* are AB839945, AB839946, and AB839947, respectively.

Alignments and phylogenetic analysis

Rodent CAT1 gene sequences were compared with other mammalian CAT1 gene sequences obtained from the DNA database: laboratory rat (*Rattus norvegicus*; AB066224) [2], laboratory mouse (*Mus musculus*; M26687) [5], human (*Homo sapiens*; X59155) [7], pig (*Sus scrofa*; AY371320) [13], domestic dog (*Canis lupus familiaris*; XM_854224) [14], American mink (*Neovison vison*; U49796) [15], domestic cat (*Felis catus*; XM_003980275) [16], chimpanzee (*Pan troglodytes*; XM_001139004), horse (*Equus caballus*; XM_001492839) [17], cattle (*Bos taurus*; NM_001135792) [18], giant panda (*Ailuropoda melanoleuca*; XM_002914759) [19], African elephant (*Loxodonta africana*; XM_0034 14018), bonobo (*Pan paniscus*; XM_003818324) [20], Syrian hamster (*Mesocricetus auratus*; U26454), Chinese hamster (*Cricetulus griseus*; U49797), orangutan (*Pongo abelii*; XM_002824135) [21], small-eared galago (*Otolemur garnettii*; XM_003797609), Northern white-cheeked gibbon (*Nomascus leucogenys*; XM_003270277), rabbit (*Oryctolagus cuniculus*; XM_002721425), lesser Egyptian jerboa (*Jaculus jaculus*; XM_004659984), naked mole rat (*Heterocephalus glaber*; XM_004854792), and degu (*Octodon degus*; XM_004631056).

The obtained three rodent CAT1 gene sequences were compared with other mammalian CAT1 gene sequences obtained from the DNA database. All the sequences were once translated into amino acids and then aligned using MUSCLE [22] implemented in MEGA ver 5.1 [23]. These aligned amino acid sequences were reversely translated into nucleotide sequences, and used for the analyses.

For phylogenetic analyses, we employed the CAT2 sequences of human (D29990) [24] and mouse (L03290) [25] for the outgroup. Therefore, we realigned all the sequences with these CAT2 sequences following the same procedure described above. A phylogenetic tree was constructed by Bayesian method. The dataset was divided into three partitions with codon position (1st, 2nd, and 3rd), and optimum substitution models for each partition were selected by Kakusan 4 [26] based on the Bayesian information criterion; general time reversible (GTR) [27] with gamma distribution (+G), GTR+G, and HKY85 [28] +G models were selected for the 1st, 2nd, and 3rd positions, respectively. The Bayesian analysis was conducted using MrBayes v3.2.1 [29] with 3 million generations of two independent runs of four Markov chains. We sampled one tree every 100 generations and calculated a consensus topology with discarding the first 25 % of trees. The final average standard deviation of split frequencies of the Bayesian analysis was 0.017942, and all average effective sample sizes were more than 200.

Statistical analysis

Differences between two groups of data were determined by the Student's *t* test. The statistical significance was set at $P < 0.05$ for all the tests.

Results

Susceptibility of rodent cells to Eco-MLV infection

Immortalized cell lines were established from the inbred southern vole (*Microtus rossiaemeridionalis*), wild large Japanese field mouse (*Apodemus speciosus*), and wild Eurasian harvest mouse (*Micromys minutus*) to assess their susceptibility to Eco-MLV infection. Cells were inoculated with the Friend MLV Env protein-carrying MLV vector, and transduction titers were measured. Infected cells were detected in the *A. speciosus* and *M. rossiaemeridionalis* cells; we observed the transduction titers for these cells to be 1/100–1/1000 times lower than those of mouse NIH3T3 cells (*M. musculus*), similar to that found on rat F10 cells (*R. norvegicus*) (Fig. 1a). In contrast, infected cells were not detected from *M. minutus*, showing that these cells are resistant to Eco-MLV infection.

To determine whether N-linked glycosylation inhibits the Eco-MLV vector infection in these rodent cells, the cells were pretreated with tunicamycin (100 μg/ml) for 24 h, and then were inoculated with the Eco-MLV vector. In the *A. speciosus, M. minutus,* and *M. rossiaemeridionalis* cells, tunicamycin treatment enhanced Eco-MLV vector infection, as in the rat F10 cells (Fig. 1b), showing that glycosylation inhibits the Eco-MLV infection in these cells. In contrast, we have already reported that tunicamycin treatment of mouse NIH3T3 cells does not affect the Eco-MLV vector infection [2, 3]. However, infection by VSV-G-pseudotyped MLV vector was not affected by the

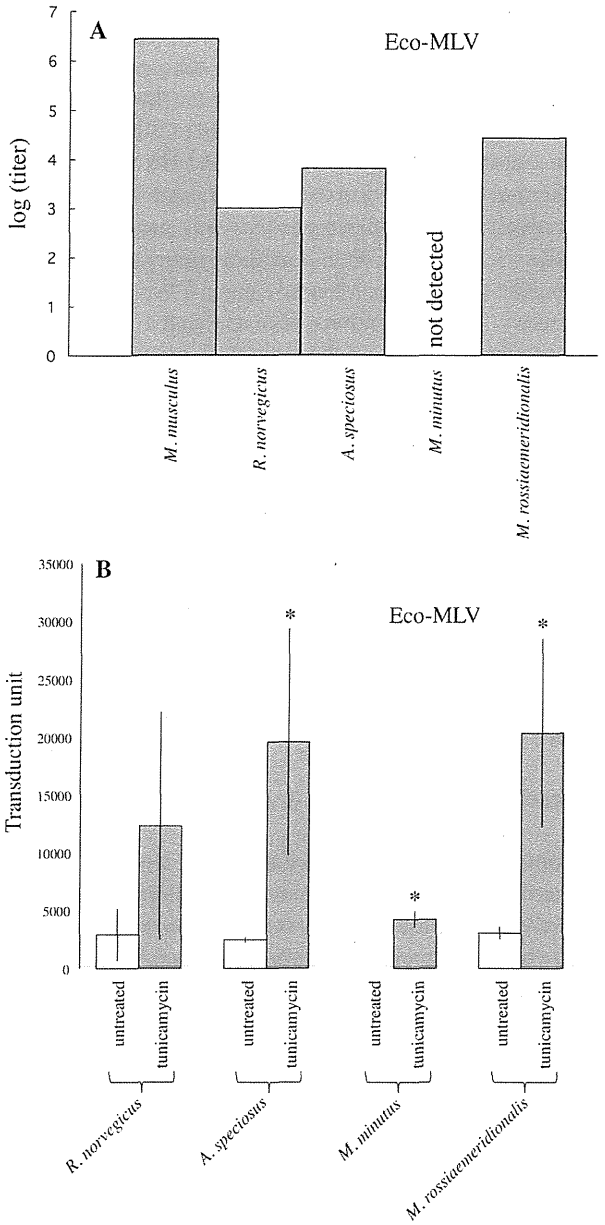

Fig. 1 Susceptibility of rodent cells to Eco-MLV infection. Rodent cells were inoculated with the Eco-MLV (**a** and **b**). Cells were treated or untreated with tunicamycin for 24 h and then were inoculated with the viral vector. These experiments were repeated three times. The results are shown as the average titers ± SD. *Asterisks* indicate statistically significant differences compared to the titer on the untreated cells

tunicamycin treatment of these cells (data not shown), suggesting that the glycosylation-mediated inhibition of MLV infection is dependent on the virus envelope protein. These data indicate that glycosylation of CAT1 proteins of *A. speciosus, M. minutus,* and *M. rossiaemeridionalis* inhibits Eco-MLV infection, suggesting that these CAT1 sequences have the amino acid insertion similar to the rat and hamster CAT1.

Nucleotide sequences of the CAT1 genes of rodent cells

DNA fragments containing the third extracellular loop and its upstream region of the CAT1 gene were isolated by RT-PCR from *M. rossiaemeridionalis, A. speciosus, and M. minutus* cells, and their nucleotide sequences were determined. Amino acid sequences of the third extracellular loop and its upstream region from the various mammals are shown in Fig. 2a, b, respectively. The CAT1 sequences of *M. rossiaemeridionalis, A. speciosus,* and *M. minutus* contain the amino acid insertions and the YGE or HGE Eco-MLV-binding motif in the third extracellular loop, as found in the hamster CAT1. Interestingly, the CAT1 sequences from rabbit (*Oryctolagus cuniculus*) and lesser Egyptian jerboa (*Jaculus jaculus*) have divergent types of deletions in the third extracellular loop.

When nucleotide sequences were compared among rodents including *M. musculus, R. norvegicus, M. minumus, A. speciosus, M. rossiaemeridionalis*, Chinese hamster (*C. griseus*), Syrian hamster (*M. auratus*), naked mole rat (*H. glaber*), degu (*O. degus*), rabbit (*O. cuniculus*), and lesser Egyptian jerboa (*J. jaculus*), the third extracellular loops (Fig. 3a) (76.4 ± 6.8 %) were less homologous than their upstream regions (Fig. 3b) (89.1 ± 4.8 %) ($P = 9.49 \times 10^{-23}$). Furthermore, the changes in the first and second nucleotides of codons in the CAT1 third extracellular loops (ECL3s) of rodents were more dominant than those in the upstream regions (Table 1), and nonsynonymous mutations in the ECL3s were more abundant than those in the upstream regions, compared to the mouse CAT1 ($P = 8.12 \times 10^{-11}$). In contrast, the amino acid sequences of the extracellular loops of the CAT1s among cat, dog, pig, horse, cattle, giant panda, elephant, small-eared galago, northern white-cheeked gibbon, Sumatran orangutan, bonobo, chimpanzee, and human are more similar than those among the rodents (Fig. 3c) (86.8 ± 7.2 %) ($P = 2.93 \times 10^{-14}$). These results suggest that the third extracellular region is under stronger selective pressure in rodents than in higher mammals.

Additionally, immortalized cells were established from inbred steppe lemming (*Lagurus lagurus*) and Mongolian gerbil (*Meriones unguiculatus*). CAT1 sequences could not be amplified from these cells by RT-PCR (data not shown). Consistently, when these cells were inoculated with the Eco-MLV vector, LacZ-expressing cells were not detected even in the presence of tunicamycin, although VSV-G-pseudotyped vector could transduce the cells. The *L. lagurus* and *M. unguiculatus* cells might be resistant due to the lack of susceptible CAT1 expression.

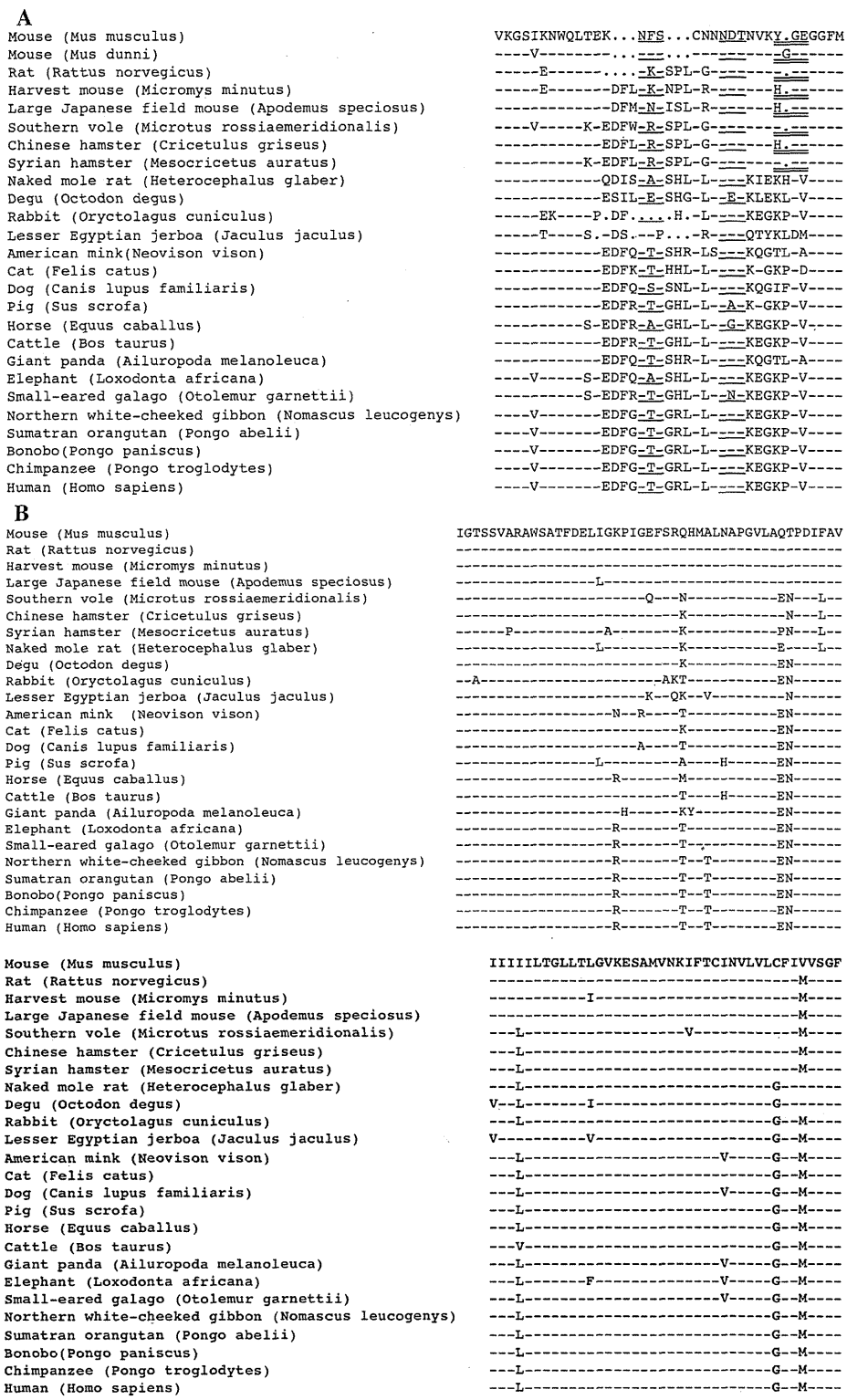

Fig. 2 Amino acid sequences of CAT1s. The amino acid sequences of the third extracellular loops (**a**) and the upstream regions (**b**) of CAT1s are indicated. *Bars* and *dots* indicate identical amino acids and deletions, respectively. N-linked glycosylation sites are *underlined*. The Eco-MLV binding motif is *double-underlined*

Fig. 3 Comparison of nucleotide sequences of CAT1s. Nucleotide sequences of the third extracellular loops (**a**) and the upstream regions (**b**) of CAT1s from indicated animals. Nucleotide sequences of the third extracellular loops (**a**) and their upstream regions (**b**) of rodent CAT1s are compared. Nucleotide sequences of the third extracellular loops of CAT1s from the higher animals are compared (**c**)

A

	M. musculus	*R.norvegicus*	*M. minutus*	*A. speciosus*	*M. rossiaemeridionalis*	*C. griseus*	*M. auratus*	*H. glaber*	*O. degus*	*O. cuniculus*	*J. jaculus*
M. musculus	100	74	76	76	71	74	74	70	72	64	66
R.norvegicus		100	82	74	82	82	82	75	74	71	69
M. minutus			100	87	76	87	82	80	79	72	69
A. speciosus				100	76	84	79	80	80	70	72
M. rossiaemeridionalis					100	89	94	81	79	68	68
C. griseus						100	94	82	80	72	72
M. auratus							100	78	77	68	68
H. glaber								100	89	72	73
O. degus									100	73	72
O. cuniculus										100	74
J. jaculus											100

B

	M. musculus	*R.norvegicus*	*M. minutus*	*A. speciosus*	*M. rossiaemeridionalis*	*C. griseus*	*M. auratus*	*H. glaber*	*O. degus*	*O. cuniculus*	*J. jaculus*
M. musculus	100	98	96	98	88	92	90	88	86	85	88
R.norvegicus		100	98	100	90	94	92	85	84	83	87
M. minutus			100	98	90	94	92	86	86	84	89
A. speciosus				100	90	94	92	84	83	84	89
M. rossiaemeridionalis					100	96	96	87	87	83	85
C. griseus						100	98	85	88	85	89
M. auratus							100	84	86	83	86
H. glaber								100	92	87	85
O. degus									100	87	89
O. cuniculus										100	86
J. jaculus											100

C

	F. catus	*C. lupus*	*S. scrofa*	*E. caballus*	*B. taurus*	*A. melanoleuca*	*L. africana*	*O. garnettii*	*N. leucogenys*	*P. abelii*	*P. paniscus*	*P. troglodytes*	*H. sapiens*
F. catus	100	79	87	79	87	82	82	82	82	82	82	82	82
C. lupus		100	79	77	82	85	82	77	79	79	79	79	79
S. scrofa			100	90	95	79	82	92	90	90	90	90	90
E. caballus				100	92	77	90	95	85	85	85	85	85
B. taurus					100	85	87	95	92	92	92	92	92
A. melanoleuca						100	79	79	77	77	77	77	77
L. africana							100	87	87	87	87	87	87
O. garnettii								100	90	90	90	90	90
N. leucogenys									100	100	100	100	100
P. abelii										100	100	100	100
P. paniscus											100	100	100
P. troglodytes												100	100
H. sapiens													100

Table 1 Changes of the first, second, and third bases of codons in mammalian CAT1s compared to mouse CAT1s

Species	Ratios of changes in upstream of ECL3 (%)			Ratios of changes in ECL3 (%)		
	First	Second	Third	First	Second	Third
R. norvegicus	0.8	0	6.9	4.0	3.4	5.1
M. minutus	0.8	0	0.5	5.1	4.5	6.2
A. speciosus	1.1	0	8.0	4.5	4.5	7.3
C. griseus	1.9	1.1	8.4	5.6	4.5	11.3
M. auratus	1.3	0.4	8.0	5.1	5.1	9.6
M. rossiaemeridionalis	3.4	0.4	9.6	5.6	5.1	11.3
H. glaber	2.7	0	9.2	6.8	6.8	16.4
O. Degus	2.7	0.4	10.7	7.3	6.8	13.6
O. cuniculus	3.8	1.1	10.0	7.9	9.0	18.6
J. jaculus	2.3	1.1	8.4	9.6	9.8	16.9

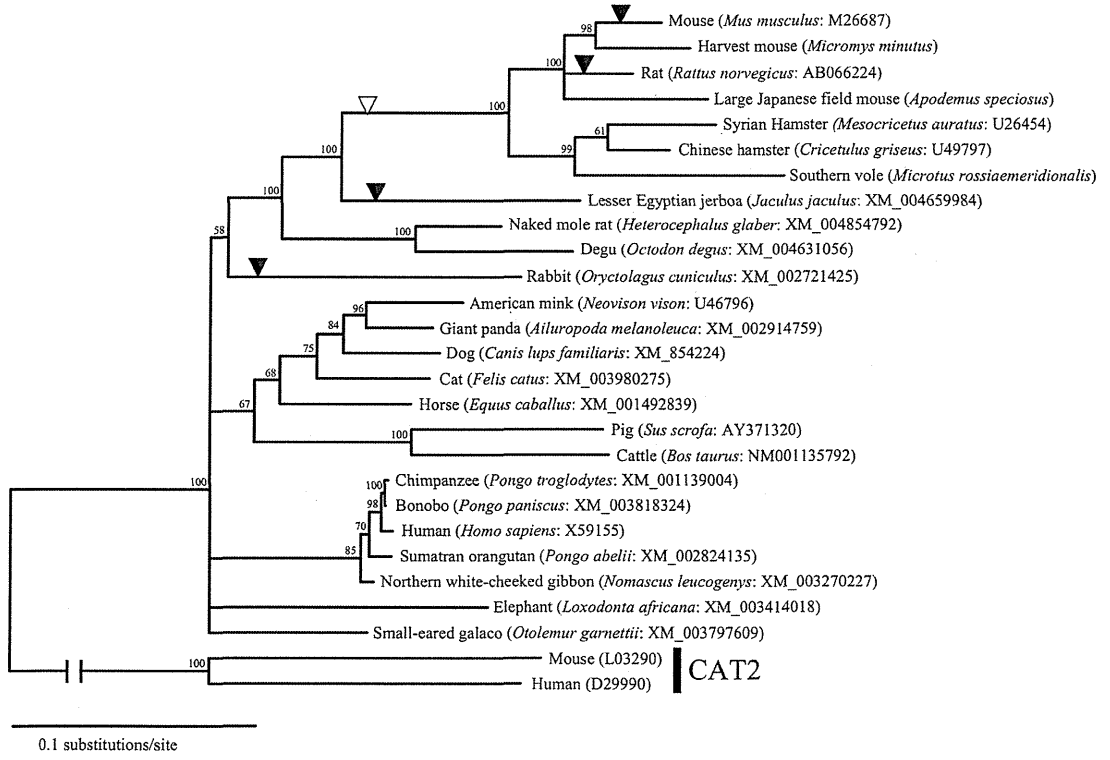

Fig. 4 Phylogenetic tree of the mammalian CAT1s. *Closed arrow heads* indicate the time points when amino acid deletions in the third extracellular loops of CAT1s occurred. An *open arrow head* shows the time point when the Eco-MLV-binding motif was obtained

Phylogenetic analysis of the ecotropic receptors

The phylogenetic tree of the CAT1s from the various mammals was constructed and is shown in Fig. 4. Rodents including mouse, rat, hamster, *A. speciosus, M. minutus*, and *M. rossiaemeridionalis* belong to one group. Human and primates belong to another group. The phylogenetic tree is consistent with the standard classification of mammals. By the phylogenetic tree, the Eco-MLV-binding motif could be obtained before mouse, rat, and hamster appeared (open arrow head in Fig. 4), and the amino acid deletions in the third extracellular loops of mouse, rat, rabbit, and lesser Egyptian jerboa CAT1s could occur independently (closed arrow heads in Fig. 4). This phylogenetic analysis also suggests that the ancestor CAT1 contain the amino acid insertion as present in the human CAT1s, and thereafter the mouse- and rat-type

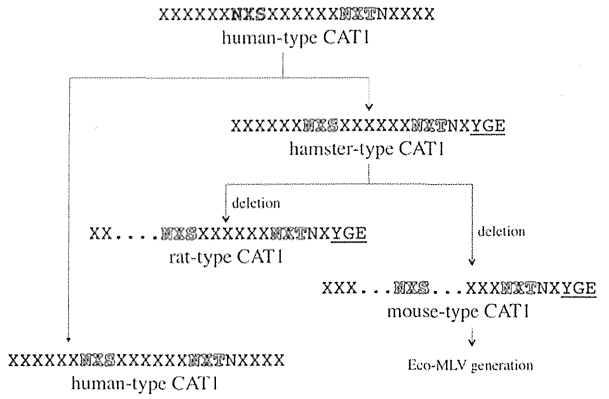

Fig. 5 Evolutionary pathway of CAT1 predicted by this study. *Block letters* show glycosylation sites. *Dots* show amino acid deletions. The Eco-MLV-binding motifs are *underlined*

CAT1s could be generated from the hamster-type CAT1 by amino acid deletion (Fig. 5).

Discussion

This study provides a putative evolution pathway of the mammalian CAT1s as follows (Fig. 5): the ancestor of the Eco-MLV receptor in mammals might not have the Eco-MLV-binding motif, like the human CAT1. Since Eco-MLV cannot infect the human CAT1, Eco-MLVs should not circulate at that time. The ancestral human-type CAT1 might be converted to the hamster-type CAT1, acquiring the virus-binding motif (open arrow head in Fig. 4). Since the hamster-type CAT1 is much less susceptible to Eco-MLV infection than the mouse CAT1, Eco-MLV should not spread at that time. The mouse CAT1 might be generated from the hamster-type CAT1 through amino acid deletion (closed arrow in Fig. 4). Since the mouse CAT1 is fully susceptible to Eco-MLV infection, Eco-MLV could circulate after the deletion occurred. Consistent with this speculation, it has been reported that many wild mice contain endogenous polytropic and xenotropic MLV sequences in their genomes but wild mice carrying the endogenous ecotropic MLV sequence are less numerous [30], suggesting that the ecotropic MLV appeared later than the polytropic and xenotropic viruses. Therefore, it is unlikely that Eco-MLV was derived from a virus which is related to Eco-MLV and efficiently interacts with the hamster-type CAT1 in the ancestor species of the *Mus* genus. Since the third extracellular loops of *Mus* subgenus animals, including *M. dunni*, *M. spicilegus*, and *M. minutoides*, have amino acid deletions as seen in the *M. musculus* CAT1 [31, 32], the deletion is thought to have occured before the *Mus* subgenus appeared.

The homology of the CAT1 third extracellular loop among the rodents is relatively lower than among the higher mammals, suggesting that the regions are under selective pressure in rodents. Since phylogenetic analysis of the mammalian CAT1s provided a possibility that Eco-MLV appeared after the *Mus* subgenus was generated, the selective pressure might not be the Eco-MLV infection itself. The CAT1 containing the amino acid deletion might be advantageous in the *Mus* subgenus, and eventually the deletion might permit the appearance of EcoMLVs. The observation that mouse, rat, rabbit, and lesser Egyptian jerboa CAT1s independently have amino acid deletions in the third extracellular loop suggests that the third extracellular loop of CAT1 is disadvantageous for rodents.

Since the one-amino acid insertion in the *Mus dunni* CAT1 is not found in the CAT1s of other *Mus* animals, it is thought that the one-amino acid insertion occurred to inhibit infection by Eco-MLV or other CAT1-recognizing viruses after the *Mus* subgenus appeared. CAT1-recognizing virus(s) might be widely spread among *M. dunni* population. To resolve this issue, further study is required.

Acknowledgments The VSV-G expression plasmid was kindly obtained from Dr. L. Chang through the AIDS Research and Reference Reagent Program, NIAID, NIH, USA. TELCeB6 cells were kindly provided by Dr. F. Cossett. We thank Ms. F. Tsujita, Ms. Y. Kobayashi, and Ms. M. Haraguchi for assistance. This study was partially supported by the Japan Society for the Promotion of Science.

References

1. Y. Huang, W.A. Paxton, S.M. Wolinsky, A.U. Neumann, L. Zhang, T. He, S. Kang, D. Ceradini, Z. Jin, K. Yazdanbakhsh, K. Kunstman, D. Erickson, E. Dragon, N.R. Landau, J. Phair, D.D. Ho, R.A. Koup, Nat. Med. **2**, 1240–1243 (1996)
2. Y. Kubo, T. Ono, M. Ogura, A. Ishimoto, H. Amanuma, Virology **303**, 338–344 (2002)
3. Y. Kubo, A. Ishimoto, T. Ono, H. Yoshii, C. Tominaga, C. Mitani, H. Amanuma, N. Yamamoto, Virology **330**, 82–91 (2004)
4. H. Yoshii, H. Kamiyama, H. Amanuma, K. Oishi, N. Yamamoto, Y. Kubo, J. Gen. Virol. **89**, 297–305 (2008)
5. L.M. Albritton, L. Tseng, D. Scadden, J.M. Cunningham, Cell **57**, 659–666 (1989)
6. L.M. Albritton, J.W. Kim, L. Tseng, J.M. Cunningham, J. Virol. **67**, 2091–2096 (1993)
7. T. Yoshimoto, E. Yoshimoto, D. Meruelo, J. Virol. **67**, 1310–1314 (1993)
8. M.V. Eiden, K. Farrell, C.A. Wilson, J. Virol. **67**, 4056–4061 (1994)
9. N. Tavoloni, A. Rudenholz, Virology **229**, 49–56 (1997)
10. F.L. Cosset, Y. Takeuchi, J.L. Battini, R.A. Weiss, M.K. Collins, J. Virol. **69**, 7430–7436 (1995)
11. Y. Kubo, A. Ishimoto, H. Amanuma, J. Virol. **77**, 7510–7516 (2003)
12. L.J. Chang, V. Urlacher, T. Iwakura, Y. Cui, J. Zucali, Gene Ther. **6**, 715–728 (1999)
13. Z. Cui, S. Zharikov, S.L. Via, S.I. Anderson, A.S. Law, A.L. Archibald, E.R. Block, Genomics **85**, 352–359 (2005)

14. K. Lindblad-Toh, C.M. Wade, T.S. Mikkelsen, E.K. Karlsson, D.B. Jaffe, M. Kamal, M. Clamp, J.L. Chang et al., Nature **438**, 803–819 (2005)
15. H. Wang, E. Klamo, S.E. Kuhmann, S.L. Kozak, M.P. Kavanaugh, D. Kabat, J. Virol. **70**, 6884–6891 (1996)
16. J.U. Pontius, J.C. Mullikin, D.R. Smith, Agencourt Sequencing team et al., Genome Res. **17**, 1675–1689 (2007)
17. C.M. Wade, E. Giulotto, S. Sigurdsson, M. Zoli, S. Gnerre, F. Imsland, T.L. Lear, D.L. Adelson, E. Bailey et al., Science **326**, 865–867 (2009)
18. A.V. Zimin, A.L. Delcher, L. Florea, D.R. Kelley, M.C. Schatz, D. Puiu, F. Hanrahan, G. Pertea, C.P. van Tassell, T.S. Sonstegard, G. Marcais, M. Roberts, P. Subramanian, J.A. Yorke, S.L. Salzberg, Genome Biol. **10**, R42 (2009)
19. R. Li, W. Fan, G. Tian, H. Zhu, L. He, J. Cai, Q. Huang, Q. Cai, B. Li, Y. Bai, Z. Zhang, Y. Zhang, W. Wang et al., Nature **463**, 311–317 (2010)
20. K. Prufer, K. Munch, I. Hellmann, K. Akagi, J.R. Miller, B. Walenz, S. Koren, G. Sutton, C. Kodira, R. Winer et al., Nature **486**, 527–531 (2012)
21. D.P. Locke, L.W. Hillier, W.C. Warren, K.C. Worley, L.V. Nararetn, D.M. Muzny, S.P. Yang, Z. Wang, A.T. Chinwalla et al., Nature **469**, 529–533 (2011)
22. R.C. Edgar, Nucleic Acid Res. **32**, 1792–1797 (2004)
23. K. Tamura, D. Peterson, N. Peterson, G. Stecher, M. Nei, S. Kumar, Mol. Biol. Evol. **28**, 2731–2739 (2011)
24. R. Hoshide, Y. Ikeda, S. Karashima, T. Matsuura, S. Komaki, T. Kishino, N. Niikawa, F. Endo, I. Matsuda, Genomics **38**, 174–178 (1996)
25. E.I. Closs, L.M. Albritton, J.W. Kim, J.M. Cunningham, J. Biol. Chem. **268**, 7538–7544 (1993)
26. A.S. Tanabe, Mol. Ecol. Resour. **11**, 914–921 (2011)
27. S. Tavaré, Some probabilistic and statistical problems in the analysis of DNA sequences, in *Some mathematical questions in biology–DNA sequence analysis*, ed. by R.M. Miura (American Mathematical Society, Providence, RI, 1986), pp. 57–86
28. M. Hasegawa, H. Kishino, T. Yano, J. Mol. Evol. **22**, 160–174 (1985)
29. F. Ronquist et al., Syst. Biol. **61**, 539–542 (2012)
30. C.A. Kozak, R.R. O'Neill, J. Virol. **61**, 3082–3088 (1987)
31. Y.T. Jung, C.A. Kozak, J. Virol. **77**, 5065–5072 (2003)
32. Y. Yan, C.A. Kozak, J. Virol. **82**, 6120–6129 (2008)

Human Mutation

OFFICIAL JOURNAL
HGVS
HUMAN GENOME VARIATION SOCIETY
www.hgvs.org

ECHS1 Mutations Cause Combined Respiratory Chain Deficiency Resulting in Leigh Syndrome

Chika Sakai,[1] Seiji Yamaguchi,[2] Masayuki Sasaki,[3] Yusaku Miyamoto,[4] Yuichi Matsushima,[1,5]* and Yu-ichi Goto[1]*

[1]*Department of Mental Retardation and Birth Defect Research, National Institute of Neuroscience, National Center of Neurology and Psychiatry, Kodaira, Tokyo, Japan;* [2]*Department of Pediatrics, Shimane University, Izumo, Shimane, Japan;* [3]*Department of Child Neurology, National Center Hospital, National Center of Neurology and Psychiatry, Kodaira, Tokyo, Japan;* [4]*Department of Pediatrics, St. Marianna University School of Medicine, Kawasaki, Kanagawa, Japan;* [5]*Department of Clinical Chemistry and Laboratory Medicine, Graduate School of Medical Sciences, Kyushu University, Fukuoka, Japan*

Communicated by David Rosenblatt

Received 4 September 2014; accepted revised manuscript 5 November 2014.
Published online 13 November 2014 in Wiley Online Library (www.wiley.com/humanmutation). DOI: 10.1002/humu.22730

ABSTRACT: The human *ECHS1* gene encodes the short-chain enoyl coenzyme A hydratase, the enzyme that catalyzes the second step of β-oxidation of fatty acids in the mitochondrial matrix. We report on a boy with ECHS1 deficiency who was diagnosed with Leigh syndrome at 21 months of age. The patient presented with hypotonia, metabolic acidosis, and developmental delay. A combined respiratory chain deficiency was also observed. Targeted exome sequencing of 776 mitochondria-associated genes encoded by nuclear DNA identified compound heterozygous mutations in *ECHS1*. ECHS1 protein expression was severely depleted in the patient's skeletal muscle and patient-derived myoblasts; a marked decrease in enzyme activity was also evident in patient-derived myoblasts. Immortalized patient-derived myoblasts that expressed exogenous wild-type ECHS1 exhibited the recovery of the ECHS1 activity, indicating that the gene defect was pathogenic. Mitochondrial respiratory complex activity was also mostly restored in these cells, suggesting that there was an unidentified link between deficiency of ECHS1 and respiratory chain. Here, we describe the patient with ECHS1 deficiency; these findings will advance our understanding not only the pathology of mitochondrial fatty acid β-oxidation disorders, but also the regulation of mitochondrial metabolism.

Hum Mutat 36:232–239, 2015.

KEY WORDS: combined respiratory chain deficiency; Leigh syndrome; ECHS1; fatty acid β-oxidation disorder

Introduction

Mitochondrial fatty acid β-oxidation provides carbon substrates for gluconeogenesis during the fasting state and contributes electrons to the respiratory chain for energy production. Once a fatty acid is activated to the acyl-coenzyme A (CoA) form and enters the mitochondrial fatty acid β-oxidation pathway, it undergoes the four following enzymatically catalyzed reaction steps during each β-oxidation cycle (Supp. Table S1): (1) dehydrogenation, (2) hydration, (3) a second dehydrogenation step, and finally (4) a thiolytic cleavage that generates one acetyl-CoA or, in certain cases, one propionyl-CoA and an acyl-CoA that is two carbons shorter than the acyl-CoA precursor. Each individual step involves specific enzymes encoded by different genes with different substrate preferences (Supp. Table S1). The first dehydrogenation reaction is catalyzed mainly by four enzymes—short-, medium-, long-, and very long chain acyl-CoA dehydrogenases (SCAD, MCAD, LCAD, and VLCAD)—with substrate optima of C4, C8, C12, and C16 acyl-CoA esters, respectively, still each dehydrogenase can utilize other suboptimal substrates [Ikeda et al., 1983, 1985a, 1985b; Ensenauer et al., 2005]. The short-chain enoyl-CoA hydratase (ECHS1) catalyzes the next step and has substrate optima of C4 2-trans-enoyl-CoA, also called crotonyl-CoA. Although ECHS1 also catalyzes hydration of medium chain substrates, longer acyl chains (e.g., C16-intermediates) are hydrated by mitochondrial trifunctional protein (MTP) [Uchida et al., 1992; Kamijo et al., 1993]. MTP consists of an alpha-subunit with long-chain enoyl-CoA hydratase and long-chain 3-hydroxyacyl-CoA dehydrogenase (LCHAD) activities and a beta-subunit with long-chain 3-ketothiolase activity.

Mitochondrial fatty acid β-oxidation disorders generally cause impaired energy production and accumulation of partially oxidized fatty acid metabolites. They are clinically characterized by hypoglycemic seizures, hypotonia, cardiomyopathy, metabolic acidosis, and liver dysfunction [Kompare and Rizzo, 2008]. The most common genetic defect in MTP is LCHAD deficiency [MIM #609016]; deficiency involving reduced activity of all three MTP enzymes [MIM #609015] is reported much less frequently and is often associated with infantile mortality secondary to severe cardiomyopathy [Spiekerkoetter et al., 2004]. Deficiency of SCAD [MIM #201470], which catalyzes the first dehydrogenation reaction and has similar substrate optima with regard to carbon chain as ECHS1, have been studied for years, and the range of associated phenotypes includes failure to thrive, metabolic acidosis, ketotic hypoglycemia, developmental delay, seizures, and neuromuscular symptoms such as myopathy and hypotonia [Jethva et al., 2008].

Additional Supporting Information may be found in the online version of this article.

*Correspondence to: Yu-ichi Goto. Department of Mental Retardation and Birth Defect Research, National Institute of Neuroscience, National Center of Neurology and Psychiatry, Kodaira, Tokyo, 187-8502, Japan. E-mail: goto@ncnp.go.jp; Yuichi Matsushima. Department of Clinical Chemistry and Laboratory Medicine, Graduate School of Medical Sciences, Kyushu University, Fukuoka, Fukuoka, 812-8582, Japan. E-mail: matsush5@cclm.med.kyushu-u.ac.jp

Contract grant sponsor(s): Grants-in-Aid for Research on Intractable Diseases (Mitochondrial Disease) from the Ministry of Health, Labor and welfare of Japan; Research Grant for Nervous and Mental Disorders from the National Center of Neurology and Psychiatry (21A-6, 24-8) and JSPS KAKENHI (25670275).

Here, we describe a patient with ECHS1 deficiency who presented with Leigh syndrome [MIM #256000] accompanied by hypotonia, metabolic acidosis, and developmental delay. Additionally, the patient presented with combined respiratory chain deficiency, which is not commonly described in most clinical reports of mitochondrial fatty acid β-oxidation disorders. Finally, we discuss the pathology of ECHS1 deficiency and possible interactions between mitochondrial fatty acid β-oxidation and the respiratory chain, which are two important pathways in mitochondrial energy metabolism.

Materials and Methods

This study was approved by the ethical committee of National Center of Neurology and Psychiatry. All the samples in this study were taken and used with informed consent from the family.

Whole-mtDNA Genome Sequence Analysis

Long and accurate PCR amplification of mtDNA followed by direct sequencing was performed according to the previous publication with a slight modification [Matsunaga et al., 2005].

Targeted Exome Sequencing

Almost all exonic regions of 776 nuclear genes (Supp. Table S2), in total 7,368 regions, were sequenced using the Target Enrichment System for next-generation sequencing (HaloPlex; Agilent Technologies, Santa Clara, California, USA) and MiSeq platform (Illumina, San Diego, California, USA). Sequence read alignment was performed with a Burrows–Wheeler Aligner (version 0.6.1) to the human reference genome (version hg19). Realignment and recalibration of base quality scores was performed with the Genome Analysis Toolkit (version 1.6.13). Variants were detected and annotated against dbSNP 135 and 1000 Genomes data (February 2012 release) by Quickannotator.

Sanger Sequencing

Sanger sequencing of candidate genes was performed with the BigDye Terminators v1.1 Cycle Sequencing kit (Thermo Fisher Scientific, Waltham, Massachusetts, USA) as per manufacturer's protocol. Details of primers and conditions are available upon request. DNA sequences from the patients were compared against the RefSeq sequence and the sequences of a healthy control or parents those were sequenced in parallel.

Cell Culture

The patient-derived primary myoblasts were established from the biopsy of patient's skeletal muscle and cultured in DMEM/F-12 (Thermo Fisher Scientific) supplemented with 20% (v/v) heat-inactivated fetal bovine serum (FBS, Thermo Fisher Scientific). DLD-1 (human colon carcinoma) cells were provided by Taiho pharmaceutical company (Tokyo, Japan) and cells were cultured in RPMI-1640 (Thermo Fisher Scientific) supplemented with 10% (v/v) heat-inactivated FBS (Thermo Fisher Scientific). All cells were cultured in 5% CO_2 at 37°C.

Preparation of Mitochondrial Fraction

Mitochondrial fractions from patient's skeletal muscle and patient-derived myoblasts were prepared according to the literature with a slight modification [Frezza et al., 2007].

Immunoblotting

Mitochondrial fraction and protein lysates were prepared from patient's skeletal muscle and patient-derived Myoblasts. Thirty micrograms of protein of mitochondrial fraction or 50 micrograms of protein lysate was separated on 4%–12% Bis-Tris gradient gels (Thermo Fisher Scientific) and transferred to polyvinylidene fluoride membranes. Primary antibodies used were against ECHS1 (Sigma-Aldrich, St. Louis, Missouri, USA), complex II 70 kDa subunit (Abcam, Cambridge, England), β-actin (Santa Cruz, Biotechnology, Dallas, Texas, USA), HA (Wako, Tokyo, Japan), and AcGFP (Thermo Fisher Scientific).

Enzyme Assays

Enzyme activities of mitochondrial respiratory complexes I–V and citrate synthase (CS) were measured in mitochondrial fraction prepared from patient's specimens. The assays for complexes I–IV and CS were performed as described previously [Shimazaki et al., 2012]. The assay for complex V was carried out following the method by Morava and his colleagues with modifications [Morava et al., 2006]. The enoyl-CoA hydratase activity was assayed by the hydration of crotonyl-CoA by a slight modification of the procedure described earlier [Steinman and Hill, 1975]. Five micrograms of protein of the mitochondrial fraction prepared from patient-derived myoblasts was added to 0.3 M Tris–HCl, pH 7.4, containing 5 mM EDTA (Ethylenediaminetetraacetic acid). The reaction was started by the addition of 200 μM crotonyl-CoA and the decrease in absorbance at 280 nm was monitored at 30°C.

Construction of the Immortalized Patient-Derived Myoblasts

The patient-derived myoblasts and control myoblasts were transfected with pEF321-T vector (A kind gift from Dr. Sumio Sugano, University of Tokyo) and the cells were cultured serially for more than ten population doublings until the morphological alteration was observed [Kim et al., 1990].

Expression Vector Preparation and Transfection

For construction of a mammalian expression vector, full-length *ECHS1* (GenBank accession number NM_004092.3) was amplified from a cDNA prepared from control subject using PrimeSTAR GXL DNA polymerase (TaKaRa, Tokyo, Japan). The PCR product was cloned into pEBMulti-Pur (Wako) and the clone was verified by Sanger sequencing. The empty expression vector or an ECHS1 expression vector was transfected into immortalized patient-derived myoblasts using Lipofectamine LTX Reagent (Thermo Fisher Scientific). Each of the two missense variants, c.2T>G; p.M1R and c.5C>T; p.A2V, was independently introduced into the clone by PCR-based site-directed mutagenesis. Each insert with C-terminal HA tag was cloned into pIRES2-AcGFP1 (Clontech Laboratories, Mountain View, California, USA) and the clones were verified by Sanger sequencing. WT and mutant ECHS1 expression vector were transfected into DLD-1 cells using Lipofectamine LTX Reagent (Thermo Fisher Scientific). Twenty-four hours later, the cell lysate was subjected to immunoblotting.

Results

The patient reported here was a boy born to unrelated, healthy parents after a 40-week pregnancy (weight 3,300 g, length 52 cm,

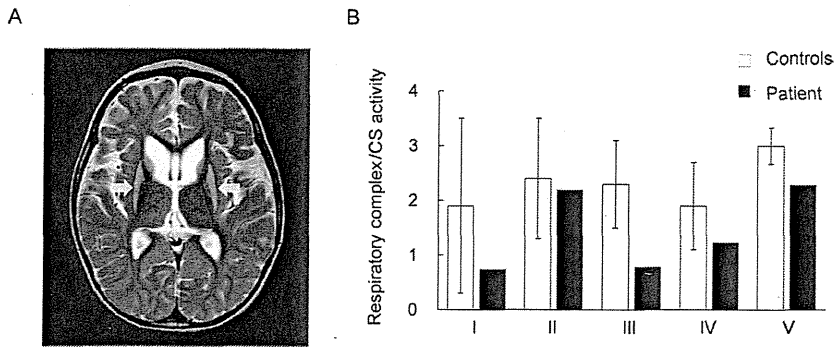

Figure 1. T2-weighted magnetic resonance scan image and enzyme activities of mitochondrial respiratory complexes. **A**: T2-weighted magnetic resonance scan image (MRI) shows bilaterally symmetrical hyperintensities in the putamen (arrows in the image); these are characteristic of Leigh syndrome. **B**: Enzymatic activities of five mitochondrial respiratory complexes (I, II, III, IV, and V) were measured in mitochondrial fractions prepared from the patient's skeletal muscle. Respiratory complexes activities were normalized to citrate synthase activity. Black bars show patient values and white bars show control values. Control values were mean values obtained from five healthy individuals. Patient activity values for complexes I, III, and IV were 39%, 34%, and 64% of the control values, respectively. Error bars represent standard deviations.

Table 1. Urinary Organic Acid Profiling

	Patient RPA (%)	Controls RPA (%)
TCA cycle intermediates		
α-Ketoglutarate	4.52	3.00–102.90
Aconitate	20.37	15.10–86.10
Isocitrate	8.98	8.30–29.00
Other metabolites		
Lactate	11.83[a]	<4.70
Pyruvate	3.18	<24.10
3-Hydroxyisobutyric acid	1.95	<9.00
Methylcitric acid	0.14[a]	Less than trace amount
p-Hydroxy-phenyllactic acid	40.05[a]	<7.00
Glyoxylate	37.71[a]	<6.10

[a]Values outside the normal range.
RPA(%), relative peak area to the area of internal standard (heptadecanoic acid, HDA).

occipitofrontal circumference (OFC) 34.5 cm). Auditory screening test at 2 months of age revealed hearing impairment, and he began to use a hearing aid at 6 months of age. Psychomotor developmental delay was noted at 5 months of age; he could not sit alone, or speak a meaningful word as of 4 years of age. Nystagmus was noted at 10 months of age. Muscle hypotonia, spasticity, and athetotic trunk movement became prominent after 1 year of age. His plasma (20.2 mg/dl) and a cerebrospinal fluid lactate were elevated (25.3 mg/dl, control below 15 mg/dl). Urinary organic acid profiling reveals significantly elevated excretion of glyoxylate (Table 1). Analysis of blood acylcarnitines showed no abnormalities. Brain magnetic resonance scan image showed bilateral T2 hyperintensity of the putamen, typical for Leigh syndrome (Fig. 1A). Because Leigh syndrome is generally caused by defects in the mitochondrial respiratory chain or the pyruvate dehydrogenase complex, we performed a muscle biopsy to measure enzyme activities of mitochondrial respiratory complexes in the patient. Mitochondrial fractions prepared from patient or control specimens were used for all activity measurements. Activity of each respiratory complex was normalized relative to CS activity; normalized values for complexes I, III, and IV activity were decreased to 39%, 34%, and 64% of control values, respectively (Fig. 1B). Moreover, we performed blue native PAGE (BN-PAGE) to examine if the assembly of respiratory complexes were altered in the patient. As a result, there were no clear difference between the patient and the control (Supp. Fig. S1).

Mitochondrial respiratory chain defects can be due to pathogenic mutations in mitochondrial DNA (mtDNA) or nuclear DNA (nDNA) coding for mitochondrial components. Initially, long and accurate PCR amplification of mtDNA followed by direct sequencing was performed and no mutations known to be associated with Leigh syndrome were identified, but previously reported polymorphisms were found (Supp. Table S3). Therefore, to identify the responsible mutations in nDNA, targeted exome sequencing was performed. Coverage was at least 10× for 86.2% of the target regions, and 30× or more for 73.4%. In all, 5,640 potential variants were identified; these included 811 splice-site or nonsynonymous variants. Among those 811 variants, 562 were on the mismapping reads that contained multiple apparent mismatches to the reference DNA sequence. Of the remaining 249 variants, nine that were on target regions with less than 10× coverage were eliminated because data reliability was low. Filtering against dbSNP 135 and 1000 Genomes data, this number was reduced to 13 including compound heterozygous variants in the *ECHS1* [MIM #602292] and 11 heterozygous variants in 11 separate genes (Supp. Table S4). Those variants have been submitted to dbSNP (http://www.ncbi.nlm.nih.gov/SNP/). Because most mitochondrial diseases caused by known nDNA mutations are inherited in an autosomal recessive manner, we focused on the compound heterozygous variants in *ECHS1*—c.2T>G; p.M1R and c.5C>T; p.A2V—as primary candidates.

To confirm the targeted exome sequencing results, we performed Sanger sequencing of genomic *ECHS1* DNA and *ECHS1* cDNA from the patient and his parents. We identified both variants, c.2T>G and c.5C>T, and the respective normal alleles in genomic DNA and cDNA from the patient (Fig. 2A and B) and no other *ECHS1* variants were detected except for common SNPs in the open reading frame. Analysis of genomic DNA from the patient's parents showed that patient's father was heterozygous for only one variant, c.2T>G, and the patient's mother for only the other variant, c.5C>T (Fig. 2A). These results indicated that the patient inherited each variant separately and that both mutant alleles were expressed in the patient (Fig. 2B). Each variant was nonsynonymous and in the region encoding the mitochondrial transit peptide (1–27 amino acids) of ECHS1 [Hochstrasser et al., 1992]; moreover, c.2T>G; p.M1R was a start codon variant (Fig. 2C).

Next, immunoblotting with primary antibodies against ECHS1 was performed to assess protein expression. Mitochondrial

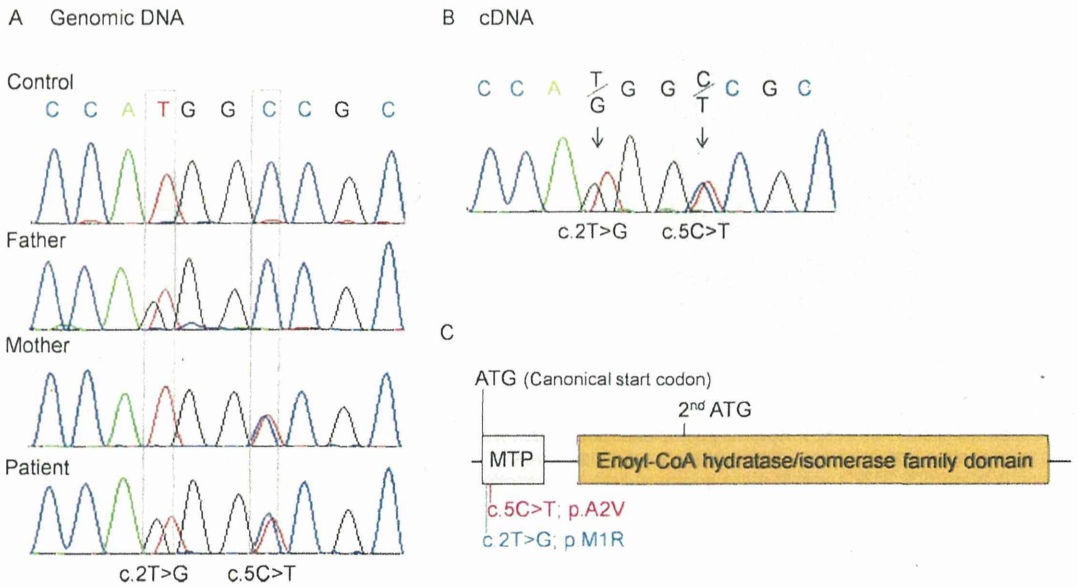

Figure 2. *ECHS1* Sanger sequencing analysis and ECHS1 functional domains. **A**: Sequence chromatograms from part of exon 1 of *ECHS1* were generated by Sanger sequencing of genomic DNA. Each parent had one wild-type allele; the patient's father also harbored a c.2T>G variant, and the patient's mother a c.5C>T variant. The patient inherited each variant allele and was a compound heterozygote. **B**: Sequence chromatograms from part of *ECHS1* exon 1 obtained by Sanger sequencing of cDNA prepared from patient mRNA. The same variants seen in genomic DNA were observed in the cDNA. **C**: A schematic diagram of the functional domains in ECHS1 and the locations of the mutations. MTP, mitochondrial transit peptide.

fractions prepared from patient and control skeletal muscle were used; whole-cell lysates or mitochondrial fractions prepared from patient-derived or control myoblasts were also used. All experiments using these specimens showed that the expression level of ECHS1 protein of the patient was too low to detect by immunoblotting even though the expression level of SDHA was almost the same as controls (Fig. 3A–C). These findings indicated that c.2T>G; p.M1R and c.5C>T; p.A2V mutations caused a remarkable reduction in ECHS1 protein expression. Notably, patient-derived and control myoblasts were similar with regard to *ECHS1* mRNA expression (Fig. 3D), indicating that the mutations apparently affected ECHS1 protein expression directly. Next, we measured ECHS1 enzyme activity in mitochondrial fractions prepared from patient-derived and control myoblasts. ECHS1 activity was normalized to CS activity, and activity in patient-derived myoblasts was 13% of that in control myoblasts (Fig. 3E). Therefore, the mutations caused a severe depletion of ECHS1 protein expression thereby decreasing ECHS1 enzyme activity.

To examine the stability of each mutated protein, we constructed three pIRES2-AcGFP1 expression plasmids, each expressed a different HA-tagged protein: wild-type, M1R-mutant, or A2V-mutant ECHS1. The expression of AcGFP was used as a transfection control. After the transfection into DLD-1 cells, immunoblotting of whole-cell lysate with anti-HA and GFP antibodies showed markedly higher expression of wild-type ECHS1 than of either mutant protein; all ECHS1 expression was normalized to AcGFP expression (Fig. 4, Supp. Fig. S2). This result indicated that ECHS1 protein expression was significantly reduced in the patient because of each mutation.

To confirm that the patient had ECHS1 deficiency, we performed a cellular complementation experiment. Patient-derived myoblasts had to be immortalized for these experiments because nonimmortalized cells exhibited poor growth and finite proliferation. The patient-derived myoblasts and control myoblasts were transfected with pEF321-T vector (a kind gift from Dr. Sumio Sugano, University of Tokyo). We then ascertained that ECHS1 protein expression and activity were lower in immortalized patient-derived myoblasts than in controls (Fig. 5A and B). We then transduced an empty expression vector, pEBMulti-Pur (Wako), or a pEBMulti-Pur construct containing a full-length, wild-type *ECHS1* cDNA into the immortalized patient-derived myoblasts; cells with the vector only or the ECHS1-expression construct are hereafter called vector-only and rescued myoblasts, respectively. ECHS1 protein expression level and enzyme activity were analyzed in mitochondrial fractions prepared from rescued myoblasts. Relative expression level of ECHS1 in rescued myoblasts was 11 times higher than that in vector-only myoblasts (Fig. 5A), and ECHS1 activity normalized to CS activity in rescued myoblasts was 49 times higher than that in vector-only myoblasts (Fig. 5B). From these cellular complementation experiments, we concluded the patient had ECHS1 deficiency.

Since the patient showed the combined mitochondrial respiratory chain deficiency in the skeletal muscle as mentioned above, we used a cellular complementation experiment to determine whether wild-type ECHS1 rescued the respiratory chain defect in patient-derived myoblasts. First, we measured enzyme activities of each mitochondrial respiratory complex in mitochondrial fractions prepared from immortalized patient-derived myoblasts. CS activity normalized values for complexes I, IV, and V activity in immortalized patient-derived myoblasts were decreased to 17%, 39%, and 43% of the mean values of immortalized control myoblasts (Fig. 5C). Then, we measured enzyme activity in mitochondrial fractions prepared from rescued myoblasts and found that each activity of complexes I, IV, and V was mostly restored relative to that in vector-only myoblasts. In rescued myoblasts, CS activity normalized values of complexes I, IV, and V were 3.5, 1.3, and 2.2 times higher than those in vector-only myoblasts (Fig. 5C). Mitochondrial respiratory complex activity was mostly restored in rescued myoblasts, suggesting that there was an unidentified link between deficiency of ECHS1 and respiratory chain.